Supporting Information

Metal-free negative linear compressibility (NLC) material - the cocrystal of 1,2-bis(4-pyridyl)ethane and fumaric acid

Ewa Patyk-Kaźmierczak,* Michał Kaźmierczak

Adam Mickiewicz University in Poznań, Uniwerystetu Poznańskiego 8, 61-614 Poznań, Poland
ewapatyk@amu.edu.pl

Table of Contents

Experimental details

1. Cocrystal synthesis

1.1. Slow evaporation

18.4 mg of 1,2-bis(4,4'-pyridyl)ethane (ETY) and 11.6 mg of fumaric acid (FUM) (1:1 mol. ratio) were dissolved in hot methanol and then left for slow evaporation. The good quality crystals emerged after couple of days (Figures S1-S3)

1.2. Solvent-assisted ball milling

61 mg of 1,2-bis(4,4'-pyridyl)ethane (ETY) and 38.9 mg of fumaric acid (FUM), ensuring 1:1 mol. ratio, were mixed and placed in a 6 ml in-house made Teflon milling cup alongside Teflon ball (5 mm in diameter) and 3 µl of 99.8% methanol (analytically pure). Sample was then milled for 15 minutes (at 30 Hz frequency) using 400 MM ball mill from Retsch. After completion of the milling sample was measured using powder X-ray diffraction.

2. X-ray diffraction experiments

2.1. Single crystal X-ray diffraction (SCXRD)

2.1.1. Ambient conditions

A single crystal (0.46x0.17x0.09 mm) suitable for SCXRD experiment was mounted on a MiTeGen loop and measured with SuperNova four-circle single crystal diffractometer from Rigaku Oxford Diffraction, equipped in mirror monochromator, micro-focus sealed X-ray tube (Cu K_α=1.54184 Å) and Atlas detector. Data were collected using CrysAlisPro[1] program at 298 K

2.1.2. High-pressure

In total three sample crystals of ETYFUM (herein labelled A, B, C; see Figures S1-S3) were selected for three series of high-pressure experiments. Each crystal was loaded in a specially prepared modified Merrill-Bassett[2] diamond anvil cell (DAC). To prepare the DAC an opening of 0.4-0.5 mm in diameter was drilled in a steel gasket (0.3 mm thick) using spark eroding machine. It was then placed in DAC and preindentation was performed to provide tight fitting of the gasket to the diamond culets and to harden the steel. A ruby chip was place in an opening (to allow pressure measurement) alongside cellulose fibres used to prevent crystal movement during the experiment (for crystals A and B). For crystal C a drop of epoxy glue was used to hold crystal in place and to allow its tilted positioning enabling collection of additional X-ray diffraction data. After sample crystal was placed in DAC the opening was covered with Daphne 7575 oil (ensuring hydrostatic conditions up to c.a. 4 GPa[3]), used as pressure-transmitting medium (PTM). The following experimental series were performed:

(i) Sample crystal A: ETYFUM was compressed up to 3.00(2) GPa and then DAC was gradually decompressed to 2.44(2), 1.85(2), 1.25(2), 0.79(2), 0.35(2) GPa with XRD measurement at each stage (Figure S1, Table S1). Sample was then compressed rapidly to 3.78(2) GPa when destruction of sample crystal was observed (Figure S1).

(ii) Sample crystal B: ETYFUM was compressed rapidly to 3.58(2) GPa directly after DAC loading, and then measured (Figure S2, Table S1).

(iii) Sample crystal C: ETYFUM was initially gradually compressed from ambient pressure and measured at 0.29(2), 0.53(2), 0.88(2), 1.33(2) GPa. After 1.33(2) GPa measurement sample was decompressed to ambient pressure and then compressed and measured at 0.08(2) and 0.15(2) GPa (Figure S3, Table S1)

Pressure was measured based on the shift of ruby fluorescence line[4] using Photon Control Inc. spectrometer (affording accuracy of about 0.02 GPa). All data were collected with four-circle single crystal Xcalibur X-ray diffractometer from Rigaku Oxford diffraction, equipped in graphite monochromator, fine-focus sealed X-ray tube (Mo K_α=0.71073 Å) and EOS CCD detector. DAC was centred using gasket shadowing method.[5] For data collection program CrysAlisPro[1] was used.

2.2. Powder X-ray diffraction (PXRD)

A sample obtained after solvent-assisted ball milling was measure using Bruker D8 Advanced diffractometer equipped in copper X-ray tube ($K_{\alpha1}$=1.5406 Å), Johnsson monochromator and LynxEye strip detector. The scan was performed for 5-50° 2ϑ angle range. Data was processed using program Kdif (from Kalvados software package[6]), and were plotted using OriginPro 2022b[7] in comparison with PXRD pattern calculated based on crystal structure of ETYFUM at 298 K/0.1 MPa using program Mercury[8] (Figure S4).

3. Crystal structure solution

Program CrysAlisPro[1] was used for *UB*-matrix determination, data reduction and absorption corrections. All crystal structures were solved either by intrinsic phasing (with ShelXT[9]) or direct methods (with ShelXS[10]). High-pressure structural models were refined with least-squares method with ShelXL[11]. For all ShelX programs Olex2[12] was used as an interface. Structure (including hydrogen atoms) at 0.1 MPa/298 K was non-spherically refined with NoSpherA2[13] implemented in Olex2,[12,14] using Orca[15] (method: PBE, basis set: cc-pVTZ, multiplicity: 2). For high-pressure structures, the hydrogen atoms were located at idealized positions based on the molecular geometry and assigned isotropic thermal parameters depending on the equivalent displacement parameters of their carriers. Due to the low number of collected data (affecting data/parameter ratio) anisotropic refinement of high-pressure structures was not possible and structures were refined isotropically. All crystal structures were deposited with the Cambridge Crystallographic Data Centre (CCDC: 2340674-2340687) and can be accessed free of charge by filling out an online form at https://www.ccdc.cam.ac.uk/structures/. Crystallographic details for all structures are listed in Table S1.

4. Principal axis strain calculations

Principal axis strain calculations for ETYFUM were performed using PASCal program[16,17] available at https://www.pascalapp.co.uk/. The ESDs on pressure values were used as weights for each data point. For the best quality data (ambient pressure crystal structure and data collected for sample crystal A) ESDs of 1 and 2 were assigned, respectively. Remaining data of poorer quality were assigned weight equal 3. All data points used for the calculations, as well as the results obtained from PASCal are collected in Tables S2-S6. An indicatrix plot showing principal axis strain is shown in Figure S5.

Where data was available, i.e., structures were deposited in Cambridge Structural Database (CSD)[18] and/or unit-cell parameters were listed in original paper, program PASCal[16,17] was used to calculate principal axis strain for other materials referenced in this work for comparison. It was done to ensure comparability of the results, by performing calculations in the same manner. Input data and the results can be found in Tables S9-S28. Our results and compressibility values reported in original publications are listed in Table S7.

In all cases a finite Eulerian strain was calculated and an empirical equation-of-state $\epsilon(p) = \epsilon_0 + \lambda(p - p_c)^v$ was fitted to the strain eigenvalues. The compressibility vs. pressure plots for all NLC materials compared in this work are shown in graph in Figure S8.

5. Compressibility capacity calculations

To calculate compressibility capacity (χ_K), functions fitted by PASCal to negative strain eigenvalues for each NLC material were exported and plotted in function of pressure. Functions were then integrated for selected minimum and maximum pressure values (for Δ*p* of 0.15, 0.9, 2.0, 3.0 GPa range, and for the total pressure range each material was investigated in) using program OriginPro[7] (the results are shown graphically in Figures S9 and S10). According to the definition of compressibility capacity: $\chi_K = -\int_{p_{min}}^{p_{max}} K(p)dp$, the area values obtained after integration need to be multiplied by -1, and discrepancy in pressure units should be taken into account (compressibility expressed in TPa^{-1} plotted in function of pressure expressed in GPa). Therefore, to express χ_K in [%], values obtained from integration were multiplied by 10^{-3} (to allow nit conversion), and by 100 to express it in [%]. All calculated values of compressibility capacity calculated in this work are listed in Table S31.

In case of $InH(BDC)_2$[19] and MIL-53(Al)[20] no information on the unit-cell parameters was provided in the original papers, and structures were not deposited in CSD. Therefore, it was not possible to calculate principal axis strain and to access the function fitted to the strain eigenvalues. However, since, both materials exhibit significant NLC it was advisable to use them as reference. Therefore, graphs from the original papers representing compressibility values were used to read the values using an online program Graph Reader (http://www.graphreader.com/). Data (listed in Tables S29 and S30) were plotted using OriginPro[7]. Function $y = a + bx^c$ was fitted to MIL-53(Al) data, and function $y = a(x - b)^c$ was fitted $InH(BDC)_2$ data, to enable integral evaluation (the exact functions are listed below Tables S29 and S30). The compressibility capacity values for all NLC materials used in comparison are shown graphically in Figure 4 in the manuscript and Figure S11.

6. CSD data-mining

The Cambridge Structural Database (version 5.45) was data-mined by original scripts using CSD Python API[18] to extract high-pressure refcode families in specific crystallographic systems (triclinic, trigonal and hexagonal; all orthogonal crystal systems, i.e. orthorhombic, tetragonal and cubic were data-mined jointly). Only families containing at least 5 refcodes of unique pressure value of measurement were taken into consideration.

7. NLC comparison

General remarks on NLC reporting and analysis: To properly asses the NLC behaviour of ETYFUM (or any other crystal) in comparison to other materials, several aspects of the manner in which data were reported in the literature need to be considered. It needs to be established and clearly disclosed whether maximal (most negative) value was given or the median (the most commonly reported value and the value produced by PASCal, a widely used principal axis strain calculator[16,17]). This will allow to avoid comparison of two values of a different meaning. Additionally, the number of experimental points, the intervals between them, and pressure range used for calculation of eigenvectors can affect the median value of compressibility. Therefore, it is important to state the pressure range the calculations were performed for, as well as the complete list of data points used, as omission or limitation of the data can shift the median to lower- or higher-pressure values, affecting reported median compressibility.

Compound used for comparison of compressibility were selected according to the following rules:

1) The results of CSD data-mining were used to create graphs representing relative changes in the unit-cell parameters to visually select crystal structures exhibiting NLC and NAC (see Table S8).

2) In case of inconclusive graphs, we have investigated whether one refcode family included more than one polymorph of given compound. In such cases data were analyzed individually for each crystal form, and only if at least 4 data points were reported for the NLC/NAC-exhibiting phase it was selected for further consideration and was included in Table S8.

3) When the same REFCODE was assigned to a crystal investigated with different PTM (eg. penetrating and non-penetrating) data were analyzed individually for each experimental series, and only if at least 4 data points were reported for the NLC/NAC-exhibiting phase it was selected for further consideration and was included in Table S8.

4) Out of the deposits found in CSD (selected according to the above-mentioned criteria) the organic crystals, crystals of organic-inorganic salts and metal complexes exhibiting NLC were selected for detailed analysis and calculation of compressibility with PASCAal[16,17] (to show how ETYFUM performs in comparison to crystals pf the similar nature).

5) Additionally, crystals described in the literature as exhibiting "giant", "colossal", "large" etc. NLC were selected for detailed analysis and calculation of compressibility capacity (if lattice constants were provided and at least 4 data points were reported either in CSD or original papers, with some exceptions described below). In some cases these structures overlapped with the structures found by data mining of CSD, but were not selected for analysis in previous steps due to the nature of the crystal.

6) If a literature source referenced an example of organic crystal exhibiting NLC of magnitude -10 TPa^{-1} and higher (i.e. more negative) it was also included in comparison, provided at least 4 data points were reported and lattice constants were provided either in CSD or original papers).

7) If structures used in analysis were deposited in CSD they are referenced by their REFCODES (Table S8). In other cases they were referenced by formulas or acronyms given in original reports.

8) In some cases (LUKWAS/LUKWOG, BIUREA I, OTELEH, YIHHON, VOFAN, LOCCAI), due to the low number of experimental points, compressibility calculations yielded highly uncertain results (strongly negative *K* values accompanied by no or extremely high ESDs). For this reason, although compressibility was initially calculated for these materials they were excluded from further analysis (including calculation of compressibility capacity) and comparison. If calculated compressibility value for the lowest pressure given material was investigated in was close to 0, but accompanied by high ESD it was included in the analysis. The exception was made for $Ag_3[Co(CN)_6]$ Phase I, CPOS-1 and water@CPOS-1, where low number of experimental data yielded results without ESDs. Still effects reported for these materials were so exceptional it was decided they should be analyzed in context of NLC in ETYFUM.

9) In total, NLC effects in 17 materials (including ETYFUM and treating each polymorph exhibiting NLC as an individual material) were used for comparison and compressibility capacity calculations.

10) For compressibility capacity comparison, the literature data reported by Cairns and Goodwin in their review[21] for some of the materials referenced by us were also included in discussion (Figures 4 and S11).

11) The following widths of pressure range were selected for compressibility capacity calculation:

- 0.15 GPa (to allow comparison to $Ag_3[Co(CN)_6]$ Phase I)
- 0.90 GPa (to allow comparison to MAGVOG I, and at the same time as 0.9 GPa is close to 1 GPa, one of the pressure limits considered relevant industrially if 0.1 MPa is considered the lower pressure limit)

- 2 GPa (the higher limit considered as industrially relevant if 0.1 MPa is considered the lower pressure limit)
- 3 GPa
- The entire pressure range each material was investigated in (according to data provided in literature)

Note these bins do not apply to all NLC materials analyzed herein, as some compounds were investigated in a pressure ranges more narrow that the ones selected.

8. Theoretical calculations

In order to assess the H-bond energy of the two types of hydrogen bonds (O-H···N and C-H···O) that play role in the molecular aggregation of the ETY and FUM molecules in ETYFUM crystal, the complexation energy was calculated (using counterpoise method) for two aggregates of the coformers (generated based on crystal structure at 298 K/0.1 MPa and shown in Table S34). Program GaussView 6.1.1,[22] Gaussian 16,[23] and hf/3-21g basis set was used for calculations. The results are listed in Table S34.

Tables

1. Experimental tables

Table S1. Experimental and crystallographic details for ETYFUM. For all structures: $C_{12}H_{12}N_2{\cdot}C_4H_4O_4$, M_r = 300.31, monoclinic, *I*2/*a*, *Z* = 4, *F*(000) = 632. Experiments were carried out at 298 K.

	etyfum	etyfum_008	etyfum_015	etyfum_029
Crystal data				
Sample crystal	N.A	C	C	C
Pressure (GPa)	0.0001(2)	0.08(2)	0.15(2)	0.29(2)
Type of experiment	N.A	Compression	Compression	Compression
a, *b*, *c* (Å)	16.6937 (2), 4.8165 (1), 19.6871 (3)	16.68 (4), 4.7884 (10), 19.65 (5)	16.72 (3), 4.7728 (7), 19.70 (4)	16.70 (3), 4.7020 (6), 19.65 (4)
β (°)	109.083 (2)	109.1 (3)	110.1 (2)	110.1 (3)
V (Å^3)	1495.96 (5)	1483 (6)	1476 (4)	1449 (5)
Radiation type	Cu *K*α	Mo *K*α	Mo *K*α	Mo *K*α
μ (mm^{-1})	0.81	0.10	0.10	0.10
Crystal size (mm)	0.46 × 0.17 × 0.09	0.33 × 0.22 × 0.03	0.33 × 0.22 × 0.03	0.31 × 0.2 × 0.03
Data collection				
Diffractometer	SuperNova, Atlas	Xcalibur, Eos	Xcalibur, Eos	Xcalibur, Eos
Absorption corr.	Analytical[a]	Gaussian[b]	Gaussian[b]	Gaussian[b]
T_{min}, T_{max}	0.799, 0.936	0.403, 0.453	0.403, 0.453	0.406, 0.452
No. of measured, independent and observed [$I > 2\sigma(I)$] reflections	12205, 1548, 1421	1576, 328, 135	1360, 315, 123	2621, 361, 171
R_{int}	0.027	0.094	0.068	0.098
$(\sin \theta/\lambda)_{max}$ (Å^{-1})	0.630	0.639	0.678	0.635
Refinement				
$R[F^2 > 2\sigma(F^2)]$, $wR(F^2)$, S	0.019, 0.052, 1.08	0.068, 0.168, 1.02	0.068, 0.169, 1.02	0.067, 0.184, 1.07
No. of reflections	1548	328	315	361
No. of parameters	173	45	45	45
No. of restraints	0	1	3	2
H-atom treatment	All H-atom parameters refined	H-atom parameters constrained	H-atom parameters constrained	H-atom parameters constrained
Weighting scheme	$w = 1/[\sigma^2(F_o^2) + (0.0264P)^2 + 0.1012P]$ where $P = (F_o^2 + 2F_c^2)/3$	$w = 1/[\sigma^2(F_o^2) + (0.0481P)^2 + 2.6463P]$ where $P = (F_o^2 + 2F_c^2)/3$	$w = 1/[\sigma^2(F_o^2) + (0.0716P)^2]$ where $P = (F_o^2 + 2F_c^2)/3$	$w = 1/[\sigma^2(F_o^2) + (0.0606P)^2 + 3.1946P]$ where $P = (F_o^2 + 2F_c^2)/3$
$\Delta\rho_{max}$, $\Delta\rho_{min}$ (e Å^{-3})	0.12, −0.10	0.17, −0.12	0.13, −0.18	0.13, −0.18

Table S1. Experimental and crystallographic details for ETYFUM. For all structures: $C_{12}H_{12}N_2{\cdot}C_4H_4O_4$, M_r = 300.31, monoclinic, *I*2/*a*, *Z* = 4, *F*(000) = 632. Experiments were carried out at 298 K- *continuation.*

	etyfum_035	etyfum_053	etyfum_079

Crystal data			
Sample crystal	A	C	A
Pressure (GPa)	0.35(2)	0.53(2)	0.79(2)
Type of experiment	Decompression	Compression	Decompression
a, *b*, *c* (Å)	16.686 (12), 4.6593 (13), 19.75 (3)	16.73 (3), 4.5924 (6), 19.74 (4)	16.758 (12), 4.5205 (17), 19.83 (2)
β (°)	110.45 (12)	110.9 (3)	111.80 (11)
V (Å^3)	1439 (2)	1417 (5)	1394 (2)
Radiation type	Mo *K*α	Mo *K*α	Mo *K*α
μ (mm^{-1})	0.10	0.10	0.10
Crystal size (mm)	0.22 × 0.19 × 0.04	0.31 × 0.2 × 0.03	0.22 × 0.19 × 0.04
Data collection			
Diffractometer	Xcalibur, Eos	Xcalibur, Eos	Xcalibur, Eos
Absorption corr.	Gaussian[b]	Analytical[a]	Gaussian[b]
T_{min}, T_{max}	0.996, 0.997	0.997, 0.998	0.995, 0.996
No. of measured, independent and observed [$I > 2\sigma(I)$] reflections	1080, 329, 180	3104, 401, 200	937, 308, 185
R_{int}	0.075	0.085	0.079
$(\sin \theta/\lambda)_{max}$ (Å^{-1})	0.622	0.639	0.604
Refinement			
$R[F^2 > 2\sigma(F^2)]$, $wR(F^2)$, S	0.089, 0.267, 1.00	0.076, 0.180, 1.03	0.085, 0.264, 1.04
No. of reflections	329	401	308
No. of parameters	46	45	46
No. of restraints	0	2	0
H-atom treatment	H-atom parameters constrained	H-atom parameters constrained	H-atom parameters constrained
Weighting scheme	$w = 1/[\sigma^2(F_o^2) + (0.1591P)^2]$ where $P = (F_o^2 + 2F_c^2)/3$	$w = 1/[\sigma^2(F_o^2) + (0.061P)^2 + 3.5496P]$ where $P = (F_o^2 + 2F_c^2)/3$	$w = 1/[\sigma^2(F_o^2) + (0.166P)^2]$ where $P = (F_o^2 + 2F_c^2)/3$
$\Delta\rho_{max}$, $\Delta\rho_{min}$ (e Å^{-3})	0.21, −0.17	0.16, −0.20	0.20, −0.17

Table S1. Experimental and crystallographic details for ETYFUM. For all structures: $C_{12}H_{12}N_2{\cdot}C_4H_4O_4$, M_r = 300.31, monoclinic, $I2/a$, Z = 4, $F(000)$ = 632. Experiments were carried out at 298 K- *continuation.*

	etyfum_088	etyfum_125	etyfum_133	etyfum_185
Crystal data				
Sample crystal	C	A	C	A
Pressure (GPa)	0.88(2)	1.25(2)	1.33(2)	1.85(2)
Type of experiment	Compression	Decompression	Compression	Decompression
a, b, c (Å)	16.72 (2), 4.4815 (7), 19.84 (3)	16.758 (8), 4.3755 (10), 19.955 (11)	16.79 (9), 4.3174 (13), 19.94 (9)	16.808 (6), 4.2460 (8), 20.027 (8)
β (°)	111.79 (18)	113.05 (6)	113.2 (6)	114.38 (5)
V (Å^3)	1380 (3)	1346.4 (11)	1329 (11)	1301.8 (8)
μ (mm^{-1})	0.11	0.11	0.11	0.11
Crystal size (mm)	0.31 × 0.2 × 0.03	0.22 × 0.19 × 0.04	0.31 × 0.2 × 0.03	0.24 × 0.20 × 0.04
Data collection				
Absorption corr.	Gaussian[b]	Gaussian[b]	Gaussian[b]	Gaussian[b]
T_{min}, T_{max}	0.397, 0.452	0.995, 0.996	0.403, 0.452	0.995, 0.996
No. of measured, independent and observed [$I > 2\sigma(I)$] reflections	2493, 420, 192	2212, 347, 228	2369, 356, 158	2475, 351, 218
R_{int}	0.102	0.083	0.142	0.088
$(\sin\theta/\lambda)_{max}$ (Å^{-1})	0.637	0.610	0.633	0.609
Refinement				
$R[F^2 > 2\sigma(F^2)]$, $wR(F^2)$, S	0.086, 0.228, 1.06	0.066, 0.192, 1.06	0.067, 0.183, 1.00	0.059, 0.198, 1.13
No. of reflections	420	347	356	351
No. of parameters	45	46	45	46
No. of restraints	2	0	1	0
Weighting scheme	$w = 1/[\sigma^2(F_o^2) + (0.0829P)^2 + 1.6991P]$ where $P = (F_o^2 + 2F_c^2)/3$	$w = 1/[\sigma^2(F_o^2) + (0.1124P)^2 + 1.7845P]$ where $P = (F_o^2 + 2F_c^2)/3$	$w = 1/[\sigma^2(F_o^2) + (0.0654P)^2]$ where $P = (F_o^2 + 2F_c^2)/3$	$w = 1/[\sigma^2(F_o^2) + (0.0998P)^2 + 1.2687P]$ where $P = (F_o^2 + 2F_c^2)/3$
$\Delta\rho_{max}$, $\Delta\rho_{min}$ (e Å^{-3})	0.15, −0.18	0.18, −0.23	0.12, −0.13	0.20, −0.21

Table S1. Experimental and crystallographic details for ETYFUM. For all structures: $C_{12}H_{12}N_2{\cdot}C_4H_4O_4$, M_r = 300.31, monoclinic, $I2/a$, Z = 4, $F(000)$ = 632. Experiments were carried out at 298 K- *continuation.*

	etyfum_244	etyfum_300	etyfum_358
Crystal data			
Sample crystal	A	A	B
Pressure (GPa)	2.44(2)	3.00(2)	3.58(2)
Type of experiment	Decompression	Compression	Compression
a, b, c (Å)	16.836 (10), 4.1496 (11), 20.120 (14)	16.874 (16), 4.0560 (16), 20.17 (2)	16.89 (5), 3.9930 (4), 20.19 (5)
β (°)	115.18 (8)	116.14 (13)	115.9 (4)
V (Å^3)	1272.0 (14)	1239 (2)	1225 (6)
μ (mm^{-1})	0.11	0.12	0.12
Crystal size (mm)	0.22 × 0.19 × 0.04	0.22 × 0.19 × 0.04	0.34 × 0.26 × 0.05
Data collection			
Absorption corr.	Analytical[a]	Gaussian[b]	Gaussian[b]
T_{min}, T_{max}	0.995, 0.996	0.995, 0.996	0.396, 0.450
No. of measured, independent and observed [$I > 2\sigma(I)$] reflections	1394, 327, 173	688, 269, 158	1236, 205, 98
R_{int}	0.091	0.089	0.083
$(\sin\theta/\lambda)_{max}$ (Å^{-1})	0.612	0.604	0.663
Refinement			
$R[F^2 > 2\sigma(F^2)]$, $wR(F^2)$, S	0.070, 0.236, 1.07	0.061, 0.157, 1.08	0.083, 0.279, 1.10
No. of reflections	327	269	205
No. of parameters	46	46	34
No. of restraints	0	0	3
Weighting scheme	$w = 1/[\sigma^2(F_o^2) + (0.1175P)^2]$ where $P = (F_o^2 + 2F_c^2)/3$	$w = 1/[\sigma^2(F_o^2) + (0.0548P)^2]$ where $P = (F_o^2 + 2F_c^2)/3$	$w = 1/[\sigma^2(F_o^2) + (0.1618P)^2]$ where $P = (F_o^2 + 2F_c^2)/3$
$\Delta\rho_{max}$, $\Delta\rho_{min}$ (e Å^{-3})	0.23, −0.31	0.14, −0.15	0.16, −0.14

[a] *CrysAlis PRO* 1.171.41.93a (Rigaku Oxford Diffraction, 2020) Analytical numeric absorption correction using a multifaceted crystal model based on expressions derived by R.C. Clark & J.S. Reid. (Clark, R. C. & Reid, J. S. (1995). Acta Cryst. A51, 887-897) Empirical absorption correction using spherical harmonics, implemented in SCALE3 ABSPACK scaling algorithm.

[b] *CrysAlis PRO* 1.171.41.93a (Rigaku Oxford Diffraction, 2020) Numerical absorption correction based on gaussian integration over a multifaceted crystal model (Absorb Angel (2004) J. Appl. Cryst. 37:486-492)

Computer programs: *CrysAlis PRO* 1.171.41.93a (Rigaku OD, 2020), SHELXT 2014/4 (Sheldrick, 2014), SHELXT (Sheldrick, 2015), *SHELXS* (Sheldrick, 2008), *SHELXL* 2014/7 (Sheldrick, 2015), Olex2 1.5 (Dolomanov *et al.*, 2009), olex2.refine 1.5 (Bourhis et al., 2015).

2. Principal axis strain calculations for ETYFUM

Table S2. Principal axis strain calculation output for ETYFUM (0.1 MPa-3.58 GPa pressure range).

			Direction			Empirical parameters			
Axes	***K* (TPa^{-1})**	**σ*K*(TPa^{-1})**	***a***	***b***	***c***	ε_0	λ	p_c	***v***
X_1	68.013	2.2443	-0.0	1.0	-0.0	152.8631	-152.8235	-1.3111	0.0009
X_2	27.8274	1.8883	0.7788	0.0	0.6273	73.4964	-73.5008	-0.9098	0.0006
X_3	-24.3616	0.9754	0.7292	0.0	-0.6843	-75.3736	75.3449	-1.6144	0.0008
V	54.0133	4.1208							

Table S3. Birch-Murnaghan coefficients for ETYFUM all data (0.1 MPa-3.58 GPa pressure range).

	B_0 (GPa)	σB_0 (GPa)	V_0 (Å^3)	σV_0 (Å^3)	B'	$\sigma B'$	p_c (GPa)
2nd	11.2529	0.4323	1487.528	5.3724	4.0	n/a	0.0
3rd	7.3076	0.8266	1498.1606	5.3212	9.1543	1.4172	0.0

Table S4. Compressibility *K* (TPa^{-1}) for ETYFUM (0.1 MPa-3.58 GPa pressure range).

***p* (GPa)**	K_1 (TPa^{-1})	K_2 (TPa^{-1})	K_3 (TPa^{-1})	σK_1 (TPa^{-1})	σK_2 (TPa^{-1})	σK_3 (TPa^{-1})
0.0001	108.9387	51.9632	-36.2692	9.7938	11.1588	5.9181
0.08	102.6872	47.7713	-34.5602	6.8996	7.3013	4.5406
0.15	97.7719	44.618	-33.1902	5.0508	4.987	3.5899
0.29	89.2302	39.415	-30.7521	2.8531	2.4037	2.2456
0.35	86.01	37.539	-29.8136	2.4141	1.9347	1.8529
0.53	77.6084	32.8489	-27.3129	2.1512	1.7655	1.1769
0.79	68.013	27.8274	-24.3616	2.2443	1.8883	0.9754
0.88	65.2219	26.429	-23.4833	2.1957	1.8422	0.9686
1.25	55.8073	21.9041	-20.4522	1.6967	1.4246	0.9118
1.33	54.1184	21.1222	-19.8969	1.57	1.3254	0.8936
1.85	45.2235	17.1447	-16.9126	1.2383	0.9978	0.8976
2.44	38.1164	14.1268	-14.4533	2.0496	1.3592	1.2517
3.0	33.1695	12.1047	-12.7005	2.9582	1.83	1.6958
3.58	29.2396	10.5419	-11.2834	3.7424	2.2297	2.1213

Table S5. The percentage change in the length of principal axes on compression (for experimental and calculated values)

p **(GPa)**	**Experimental**			**Calculated**		
	X_1 **(%)**	X_2 **(%)**	X_3 **(%)**	$X_{1,calc}$ **(%)**	$X_{2,calc}$ **(%)**	$X_{3,calc}$ **(%)**
0.0001	-0.0	0.0	0.0	0.0921	0.0008	-0.0591
0.08	-0.5851	-0.199	-0.082	-0.7528	-0.3972	0.2237
0.15	-0.9114	-1.1396	0.7471	-1.4542	-0.7203	0.4608
0.29	-2.4055	-1.3324	0.5671	-2.7614	-1.3071	0.9079
0.35	-3.317	-1.562	1.003	-3.287	-1.5378	1.0896
0.53	-4.7607	-1.997	1.3788	-4.7569	-2.1694	1.6031
0.79	-6.3336	-2.8143	2.2615	-6.6445	-2.9546	2.2734
0.88	-7.1958	-2.9072	2.1795	-7.2439	-3.1987	2.4886
1.25	-9.5709	-4.1065	3.3915	-9.4739	-4.0876	3.2989
1.33	-10.892	-4.2173	3.5308	-9.9135	-4.2597	3.4602
1.85	-12.5335	-5.4633	4.5663	-12.4826	-5.2474	4.4131
2.44	-14.78	-6.1948	5.4055	-14.9292	-6.1642	5.3346
3.0	-16.9922	-7.1966	6.2631	-16.9188	-6.8958	6.0928
3.58	-18.4969	-6.7909	6.2034	-18.7238	-7.5504	6.7867

Table S6. Input data for calculations for ETYFUM all data (0.1 MPa-3.58 GPa pressure range).

p **(GPa)**	***σp*** **(GPa)**	***a*** **(Å)**	***b*** **(Å)**	***c*** **(Å)**	***α*** **(º)**	***β*** **(º)**	***γ*** **(º)**
0.0001	1.0	16.6937	4.8165	19.6871	90.0	109.083	90.0
0.08	3.0	16.68	4.7884	19.65	90.0	109.1	90.0
0.15	3.0	16.72	4.7728	19.7	90.0	110.1	90.0
0.29	3.0	16.7	4.702	19.65	90.0	110.1	90.0
0.35	2.0	16.686	4.6593	19.75	90.0	110.45	90.0
0.53	3.0	16.73	4.5924	19.74	90.0	110.9	90.0
0.79	2.0	16.758	4.5205	19.83	90.0	111.8	90.0
0.88	3.0	16.72	4.4815	19.84	90.0	111.79	90.0
1.25	2.0	16.758	4.3755	19.955	90.0	113.05	90.0
1.33	3.0	16.79	4.3174	19.94	90.0	113.2	90.0
1.85	2.0	16.808	4.246	20.027	90.0	114.38	90.0
2.44	2.0	16.836	4.1496	20.12	90.0	115.18	90.0
3.0	2.0	16.874	4.056	20.17	90.0	116.14	90.0
3.58	3.0	16.89	3.993	20.19	90.0	115.9	90.0

3. Details on Negative Linear Compressibility (NLC) in selected materials

3.1. Lists of NLC materials selected from literature and found in CSD

Table S7. Reported and calculated NLC values for selected NLC materials.

Crystal (REFCODE)	Median compressibility	
	Reported	Calculated in this work

	K (TPa^{-1})	Δp (GPa)	ref	K (TPa^{-1})	Δp (GPa)
ETYFYM				-24.36(98)	0.0001-3.58
$Ag_3[Co(CN)_6]$ Phase I	-76(9)	0.0001-0.157	[24]	-72	0.0001-0.15
$Ag_3[Co(CN)_6]$ Phase II	-5.3(3)	0.19-7.65	[24]	-11.91(64)	0.19-7.65
$[Ag(en)]NO_3$-I (MAGVOG)	-28.4(18)	0.0001-0.92	[25]	-28.3(22)	0.0001-0.92
Lithium L-tartrate (UNIRUF)	-16(2)	2.01-5.52	[26]	-15.4(15)	2.01-5.52
BTCP·dItFB (LUKWAS/LUKWOG)	-30	0.0001-0.7	[27]	-4.5(15)	0.0001-2.5
$(C_6F_5Au)_2$(μ-1,4-diisocyanobenzene) (JOHGIX)	-12.6(25)	0.0001-2.42	[28]	-18.8(24)	0.0001-4.39
$Zn[Au(CN)_2]_2$ Phase I	-42(5)	0.35-1.78	[29]	-37.1(42)	0.35-1.78
$Zn[Au(CN)_2]_2$ Phase II	-6(3)	2.04-14.22	[29]	-4.5(10)	2.04-14.22
SULBAC	Not reported	0.91-2.83	[30]	-5.9(11)	0.91-2.83
BIUREA I	-2.7(5)	0.0001-0.5	[31]	-5(30)	0.0001-0.5
BIUREA II[c]	-0.856(2)	0.62-3.89	[31]	-4.6(5)	0.62-2.81
POWSID	-41	0.0001-0.48	[32]	-16.4(35)	0.0001-2.48
QAXMEH	-5.5(8)	0.54-2.84	[33]	-5.4(15)	0.54-2.84
CPOS-1	~ -20[a] (-90.7)	1.02-2.32 (At 2.32)	[34]	-22.7	1.02-2.32
WATER@CPOS-1[b]	-13.3	0.58-2.53	[34]	-8.0	0.58-2.53
$InH(BDC)_2$	-62.4	0-0.53	[19]		
MIL-53(Al) I	-7.7	0-1.8	[20]		

[a] value not listed, value read form the Graph in Figure 2 of the original paper [ref]

[b] The pressure range used for calculation in original work yielded highly biased values (very high ESD for all values), probably due to the same length of the unit-cell parameter *c* (i.e. direction exhibiting NLC) for the last two pressure points; therefore for calculations in this work the data point at 1.96 GPa was omitted from calculations (omitting the last point i.e. at 2.53 GPa led to software crash and principal axes could not be calculated)

[c] The tendency in the pressure-dependence of the length of parameter *c* (lying close to the principal axis exhibiting NLC) changed above 2.81, therefore data points above that pressure were omitted (including them led to function yielding biased values of compressibility)

Table S8. List of RFCODE families for crystal structures deposited in CSD, where NLC or NAC was observed found by datamining. Crystals were divided based on the type of the crystal: organic, organic-inorganic salts, metal complexes, coordination polymers (including MOFs- refcodes in bold font). The crystal system is denoted by the first letter of the appropriate system: m-monoclinic, o-orthorhombic, t-tetragonal, hexagonal.

Refcode	Crystal system	Ref.	Additional information	Formula	Compound name
ORGANIC					
BIUREA	m	31	NLC in Phase I and II	$C_2D_6N_4O_2$	perdeuterohydrazine-1,2-dicarboxamide
EGEWEV	o	35	NLC[a]	$C_7H_5NO,x(He)$	4-hydroxybenzonitrile helium
KOWYEA	o	36	NAC in *β* polymorph	$C_8H_8N_2$	2-methyl-1H-benzimidazole
LOCCAI	m	37	NLC in H1 polymorph	$C_{12}H_{17}N_2S^+,Cl^-,H_2O$	2-((2,6-dimethylphenyl)amino)-5,6-dihydro-4H-1,3-thiazin-3-ium chloride monohydrate
QAXMEH	m	33	NLC in yellow polymorph	$C_{12}H_9N_3O_2S$	5-Methyl-2-((2-nitrophenyl)amino)-3-thiophenecarbonitrile
VOFVAN	m	38	NLC above 1GPa	$C_{13}H_{11}NO$	4-Aminobenzophenone
YIHHON	o	39	NLC above 2.5 GPa	$C_3H_7NO_2$	2-(Methylamino)acetic acid
ORGANIC-INORGANIC SALTS					
IZIYOI	m	40	NLC in high-pressure phase	$C_6H_{13}N_2^+,H_2NO_3S^-,H_2O$	1,4-diazabicyclo[2.2.2]octan-1-ium sulfamate monohydrate
OTELEH	m	41	NLC	$C_2H_6NO_2^+,H_2O_3P^-$	glycinium hydrogen phosphite
METAL COMPLEXES					
JOHGIX	m	28	NLC	$C_{20}H_4Au_2F_{10}N_2$	(μ_2-1,4-Di-isocyanobenzene)-bis(pentafluorophenyl)-di-gold
POWSID	m	32	NLC	$C_{38}H_{20}FeN_{10}S_2,C_5H_5N$	bis(Dipyrido(3,2-a:2',3'-c)phenazine)-di-isothiocyanato-iron(ii) pyridine solvate
SULBAC	t	30	NLC	$C_{56}H_{84}O_4Th$	tetrakis(2,6-di-t-butylphenolato)-thorium(iv)
COORDINATION POLYMERS (including **MOFs**)					
CEGFEA	m	42	NLC in phase I and II	$(C_8H_{10}Ag_2N_4)_n$	catena-((μ_2-2-Methylimidazole-N,N')-silver(i))
FUVDEH[b]	**t**	43	**NAC**	**$(C_{18}H_{12}N_2O_3Zn)_n,n(H_2O)$**	**catena-[(μ_2-4-(1H-Naphtho[2,3-d]imidazol-1-yl)benzoato)-(μ_2-hydroxo)-zinc(ii) monohydrate]**
IFEPUG[b]	**t**	43	**NAC**	**$(C_{18}H_{12}N_2O_3Zn)_n,n(CH_4O)$**	**catena-[(μ_2-Hydroxo)-(μ_2-4-(1H-naphtho[2,3-d]imidazol-1-yl)benzoato)-zinc methanol solvate]**
JEXWOZ	**m**	44	**NLC in AMnF-II**	**$(C_3H_3MnO_6^-)_n,n(H_4N^+)$**	**catena-(ammonium tris(μ_2-formato)-manganese(ii))**
JEXXAM	h	45	NLC	$(C_3H_3NiO_6^-)_n,H_4N^+$	catena-[ammonium tris(μ-formato)-nickel]
MAGVOG	**m**	25	**NLC in Phase I**	**$(C_2H_8AgN_2^+)_n,n(NO_3^-)$**	**[Ag(en)]NO_3-I (catena-((m2-Ethylene-1,2-diamine-N,N')-silver(i) nitrate))**
NEVSUF	**t**	46	**NLC**	**$(C_{46}H_{42}O_{16}Zr_3)_n$**	**catena-[tetrakis(μ-hydroxo)-(μ-3,3',5,5'-tetrakis(4-carboxylatophenyl)-2,2',4,4',6,6'-hexamethyl-1,1'-biphenyl)-tetrakis(hydroxy)-tri-zirconium unknown solvate]**
NEVTIU	**t**	46	**NLC**	**$(C_{46}H_{42}Hf_3O_{16})_n$**	**catena-[tetrakis(μ-hydroxo)-(μ-3,3',5,5'-tetrakis(4-carboxylatophenyl)-2,2',4,4',6,6'-hexamethyl-1,1'-biphenyl)-tetrakis(hydroxy)-tri-hafnium(iv) unknown solvate]**
OVUFAP	**m**	47	**NLC of *β*-AMU3·DMF compressed in methanol:ethanol:water**	**$(C_{18}H_{12}CdN_4O_4)_n,C_3H_7NO$**	**catena-[(μ-terephthalato)-(μ-4,4'-diazenediyldipyridine)-cadmium(ii) N,N-dimethylformamide solvate]**
UNIRUF	m	26	NLC in phase II	$(C_8H_8Li_4O_{12})_n$	catena-[bis(μ-dihydrogen-L-tartrato)-tetra-lithium]
YOLKOB	**o**	48	**NLC when non-penetrating medium is used (glicerin and daphne oil 7474)**	**$(C_{39}H_{24}F_6N_2O_4S_2Zn)_n$, $2n(C_3H_7NO)$, $n(H_2O)$**	**catena-[(μ_2-4,4'-((3,3,4,4,5,5-hexafluorocyclopent-1-ene-1,2-diyl)bis(5-methylthiene-4,2-diyl))dipyridine)-(μ_2-biphenyl-4,4'-dicarboxylato)-zinc N,N-dimethylformamide solvate monohydrate]**

3.2. Principal axis strain calculation for selected NLC materials

Table S9. Principal axis strain calculation details for CPOS-1.[34]

Input data							
p **(GPa)**	**σ*p* (GPa)**	***a*** **(Å)**	***b*** **(Å)**	***c*** **(Å)**	***α*** **(º)**	***β*** **(º)**	***γ*** **(º)**
1.02	1.0	23.48	23.48	7.1	90.0	90.0	90.0
1.4	1.0	23.37	23.37	7.12	90.0	90.0	90.0
1.82	1.0	23.2	23.2	7.24	90.0	90.0	90.0
2.32	1.0	22.81	22.81	7.49	90.0	90.0	90.0

Principal axis strain calculation output									
			Direction			**Empirical parameters**			
Axes	***K*** **(TPa^{-1})**	**σ*K*(TPa^{-1})**	***a***	***b***	***c***	ε_0	***λ***	p_c	***v***
X_1	14.0516	nan	1.0	0.0	-0.0	0.0065	-0.0	-63.5481	83.8857
X_2	14.0516	nan	0.0	1.0	0.0	0.0065	-0.0	-63.5481	83.8857
X_3	-22.6971	nan	-0.0	-0.0	1.0	-0.0005	0.0312	1.02	2.0913
V	2.3821	1.9441							

Birch-Murnaghan coefficients							
	B_0 **(GPa)**	σB_0 **(GPa)**	V_0 **(Å^3)**	σV_0 **(Å^3)**	***B'***	***σB'***	p_c **(GPa)**
2nd	90.4371	125.6994	3968.0243	94.2254	4.0	n/a	0.0
3rd	835.0298	237.3798	3919.8593	3.1092	-194.0821	35.0304	0.0
3rd with P_c	604.2267	205.0766	3914.3087	2.2661	-270.9185	40.017	1.02

Compressibility						
p **(GPa)**	K_1 **(TPa^{-1})**	K_2 **(TPa^{-1})**	K_3 **(TPa^{-1})**	σK_1 **(TPa^{-1})**	σK_2 **(TPa^{-1})**	σK_3 **(TPa^{-1})**
1.02	8.6397	8.6397	-0.0	nan	nan	nan
1.4	14.0516	14.0516	-22.6971	nan	nan	nan
1.82	23.9749	23.9749	-51.1449	nan	nan	nan
2.32	45.0868	45.0868	-86.8783	nan	nan	nan

Comments

An unusual behaviour of unit-cell volume of dry CPOS-1 can be noticed between 1.4 and 2.3 GPa, where a slight increase and then stabilization of its value is observed, an occurrence not addressed by the authors of original report. Noteworthy, provided crystal structures were simulated with Density Functional Theory calculations rather than solved based on experimental data. This, alongside the lack of the ESDs on the reported volume values and no access to experimental data that would enable revision of the reported structures, make it hard to explain this very unusual behaviour. There are examples in the literature where porous crystals increased their volume at high pressure, but it was due to the adsorption of the molecules of pressure transmitting medium (PTM).[49] In case of the CPOS-1 silicon oil was used as PTM, which is considered non-penetrating medium, but it is not unheard of for fragments of the framework destroyed by pressure to be forced in the pores, expanding the crystal structure.[50] It is also possible for the PTM to be contaminated with compounds of smaller molecules, such as water.[27] In such case the composition of the crystal changes, and it is hard to consider expansion as NLC.

Table S10. Principal axis strain calculation details for water@CPOS-1.[34]

Input data							
p **(GPa)**	**σ*p* (GPa)**	***a*** **(Å)**	***b*** **(Å)**	***c*** **(Å)**	***α*** **(º)**	***β*** **(º)**	***γ*** **(º)**
0.58	1.0	23.83	23.83	7.12	90.0	90.0	90.0
0.98	1.0	23.68	23.68	7.13	90.0	90.0	90.0
1.32	1.0	23.57	23.57	7.16	90.0	90.0	90.0
2.53	1.0	22.02	22.02	7.27	90.0	90.0	90.0

Principal axis strain calculation output									
			Direction			**Empirical parameters**			
Axes	***K*** **(TPa^{-1})**	**σ*K*(TPa^{-1})**	***a***	***b***	***c***	ε_0	***λ***	p_c	***v***
X_1	14.882	nan	1.0	0.0	-0.0	0.0061	-0.0	-62.8572	84.0623
X_2	14.882	nan	-0.0	1.0	-0.0	0.0061	-0.0	-62.8572	84.0623
X_3	-8.0039	nan	0.0	0.0	1.0	-0.0002	0.0083	0.58	1.4066
V	68.8689	6.9251							

Birch-Murnaghan coefficients							
	B_0 **(GPa)**	σB_0 **(GPa)**	V_0 **(Å^3)**	σV_0 **(Å^3)**	***B'***	***σB'***	p_c **(GPa)**
2nd	6.3487	2.3015	4508.5645	214.4516	4.0	n/a	0.0
3rd	49.3978	8.5151	4090.7561	15.518	-5.5174	0.7153	0.0
3rd with P_c	45.8784	8.1177	4041.288	7.7744	-6.6775	0.6811	0.58

Compressibility						
p **(GPa)**	K_1 **(TPa^{-1})**	K_2 **(TPa^{-1})**	K_3 **(TPa^{-1})**	σK_1 **(TPa^{-1})**	σK_2 **(TPa^{-1})**	σK_3 **(TPa^{-1})**
0.58	8.8291	8.8291	-0.0	Nan	nan	nan
0.98	14.882	14.882	-8.0039	Nan	nan	nan
1.32	23.1356	23.1356	-10.2784	Nan	nan	nan
2.53	109.1642	109.1642	-15.2409	Nan	nan	nan

Table S11. Principal axis strain calculation details for BIUREA I.[31]

Input data							
p **(GPa)**	***σp*** **(GPa)**	***a*** **(Å)**	***b*** **(Å)**	***c*** **(Å)**	***α*** **(º)**	***β*** **(º)**	***γ*** **(º)**
0.0001	1.0	9.3308	4.6415	11.4721	90.0	82.069	90.0
0.02	1.0	9.337	4.6053	11.4184	90.0	82.134	90.0
0.026	1.0	9.338	4.5938	11.4034	90.0	82.154	90.0
0.36	1.0	9.3394	4.5765	11.3816	90.0	82.16	90.0
0.5	1.0	9.3429	4.555	11.3567	90.0	82.183	90.0

Principal axis strain calculation output									
			Direction			**Empirical parameters**			
Axes	***K*** **(TPa^{-1})**	***σK*** **(TPa^{-1})**	***a***	***b***	***c***	ε_0	***λ***	p_c	***v***
X_1	75.9714	271.8308	0.0	1.0	-0.0	0.0002	-0.0202	0.0001	0.2112
X_2	39.1429	134.9569	0.0484	0.0	0.9988	0.0002	-0.0108	0.0001	0.1823
X_3	-5.28	28.1664	0.9899	0.0	-0.142	-0.0001	0.0017	0.0001	0.1362
V	37.2064	8.4055							

Birch-Murnaghan coefficients							
	B_0 **(GPa)**	σB_0 **(GPa)**	V_0 **(Å^3)**	σV_0 **(Å^3)**	***B'***	***σB'***	p_c **(GPa)**
2nd	18.9238	6.6524	489.232	2.2319	4.0	n/a	0.0
3rd	11.0577	12.2762	487.3255	2.5978	190.9448	203.8862	0.0

Compressibility						
p **(GPa)**	K_1 **(TPa^{-1})**	K_2 **(TPa^{-1})**	K_3 **(TPa^{-1})**	σK_1 **(TPa^{-1})**	σK_2 **(TPa^{-1})**	σK_3 **(TPa^{-1})**
0.0001	$454*10^6$	$334*10^6$	$-18*10^6$	$33*10^{12}$	$15*10^{12}$	$156*10^9$
0.02	93.5252	48.5555	-6.6297	392.8542	196.9653	41.7619
0.026	75.9714	39.1429	-5.28	271.8308	134.9569	28.1664
0.36	9.5305	4.5509	-0.5438	25.8439	12.298	2.3988
0.5	7.3544	3.4786	-0.4094	25.6359	12.0346	2.2978

Table S12. Principal axis strain calculation details for BIUREA II.[31]

Input data							
p **(GPa)**	***σp*** **(GPa)**	***a*** **(Å)**	***b*** **(Å)**	***c*** **(Å)**	***α*** **(º)**	***β*** **(º)**	***γ*** **(º)**
0.62	1	9.4872	3.81402	12.8589	90.0	77.936	90.0
0.9	1	9.485	3.70468	12.9889	90.0	77.632	90.0
1.31	1	9.4768	3.61125	13.0677	90.0	77.463	90.0
1.63	1	9.4644	3.5503	13.1017	90.0	77.388	90.0
1.87	1	9.4568	3.51779	13.1178	90.0	77.346	90.0
2.02	1	9.4526	3.49778	13.1229	90.0	77.341	90.0
2.25	1	9.4444	3.46902	13.1315	90.0	77.318	90.0
2.53	1	9.4344	3.44007	13.1345	90.0	77.317	90.0
2.81	1	9.4251	3.41438	13.1382	90.0	77.309	90.0

Principal axis strain calculation output									
			Direction			**Empirical parameters**			
Axes	***K*** **(TPa^{-1})**	***σK*** **(TPa^{-1})**	***a***	***b***	***c***	ε_0	***λ***	p_c	***v***
X_1	38.2921	0.3944	0.0	1.0	-0.0	0.1962	-0.251	0.2976	0.2174
X_2	3.9343	0.0721	0.9748	0.0	-0.2229	0.0001	-0.0047	0.6097	0.8679
X_3	-4.6498	0.4562	0.1447	-0.0	0.9895	-35.6587	35.6765	0.5685	0.0002
V	41.9047	2.764							

Birch-Murnaghan coefficients							
	B_0 **(GPa)**	σB_0 **(GPa)**	V_0 **(Å^3)**	σV_0 **(Å^3)**	***B'***	***σB'***	p_c **(GPa)**
2nd	16.3976	0.7431	468.8453	1.7321	4.0	n/a	0.0
3rd	0.0541	112.807	507.0226	702.0038	1495.1378	3100231.2846	0.0
3rd with P_c	12.7127	0.4962	454.9202	0.358	12.7071	0.8918	0.62

Compressibility						
p **(GPa)**	K_1 **(TPa^{-1})**	K_2 **(TPa^{-1})**	K_3 **(TPa^{-1})**	σK_1 **(TPa^{-1})**	σK_2 **(TPa^{-1})**	σK_3 **(TPa^{-1})**
0.62	132.3306	7.4259	-117.3541	8.804	12.3115	83.4761
0.9	81.1335	4.7764	-18.2496	1.0188	0.2933	3.4628
1.31	54.0445	4.2519	-8.1605	0.8198	0.1392	1.0576
1.63	43.5914	4.0456	-5.7008	0.4621	0.0753	0.5672
1.87	38.2921	3.9343	-4.6498	0.3944	0.0721	0.4562
2.02	35.6567	3.8763	-4.1694	0.4471	0.0844	0.4356
2.25	32.3251	3.7997	-3.5992	0.5781	0.1099	0.4327
2.53	29.1065	3.7214	-3.0855	0.7391	0.1414	0.4426
2.81	26.5356	3.6551	-2.7001	0.8759	0.1703	0.4521

Table S13. Principal axis strain calculation details for QAXMEH. [33]

Input data							
p **(GPa)**	***σp*** **(GPa)**	***a*** **(Å)**	***b*** **(Å)**	***c*** **(Å)**	***α*** **(º)**	***β*** **(º)**	***γ*** **(º)**
0.54	1	8.337	15.8027	8.4626	90.0	91.44	90.0
0.99	1	8.2031	15.4235	8.4569	90.0	90.851	90.0
1.49	1	8.116	15.121	8.4699	90.0	90.38	90.0
1.89	1	8.0755	14.874	8.4734	90.0	89.76	90.0
2.84	1	8.0025	14.448	8.4923	90.0	89.15	90.0

Principal axis strain calculation output									
			Direction			**Empirical parameters**			
Axes	***K*** **(TPa^{-1})**	***σK*** **(TPa^{-1})**	***a***	***b***	***c***	ε_0	***λ***	p_c	***v***
X_1	38.7817	2.2201	0.0	1.0	-0.0	0.0782	-0.0975	-0.1051	0.5018
X_2	19.4573	0.624	0.9611	0.0	-0.276	49.4556	-49.4741	0.0179	0.0006
X_3	-5.3689	1.5158	0.304	0.0	0.9527	-0.0003	0.0048	0.54	1.138
V	50.2775	5.3564							

Birch-Murnaghan coefficients							
	B_0 **(GPa)**	σB_0 **(GPa)**	V_0 **(Å^3)**	σV_0 **(Å^3)**	***B'***	***σB'***	p_c **(GPa)**
2nd	12.5247	1.2031	1150.7838	10.3148	4.0	n/a	0.0
3rd	0.0126	576.9656	1263.2294	14753.7505	3899.8433	177534163.3117	0.0
3rd with P_c	8.7955	0.6861	1114.2898	2.1374	13.0842	1.4655	0.54

Compressibility						
p **(GPa)**	K_1 **(TPa^{-1})**	K_2 **(TPa^{-1})**	K_3 **(TPa^{-1})**	σK_1 **(TPa^{-1})**	σK_2 **(TPa^{-1})**	σK_3 **(TPa^{-1})**
0.54	60.8826	54.8297	-0.0339	13.9939	6.338	$40*10^{12}$
0.99	46.7732	29.4583	-4.8428	2.3386	1.0441	3.3248
1.49	38.7817	19.4573	-5.3689	2.2201	0.624	1.5158
1.89	34.6908	15.3021	-5.6357	1.2206	0.5081	0.8538
2.84	28.5728	10.1533	-6.0658	3.229	0.9028	2.387

Table S14. Principal axis strain calculation details for IZIYOI hp.[40]

Input data							
p **(GPa)**	**σ*p* (GPa)**	***a*** **(Å)**	***b*** **(Å)**	***c*** **(Å)**	***α*** **(º)**	***β*** **(º)**	***γ*** **(º)**
1.36	1	5.2002	14.798	12.423	90.0	96.112	90.0
1.51	1	5.1961	14.805	12.343	90.0	96.0	90.0
1.65	1	5.1914	14.812	12.293	90.0	95.93	90.0
1.73	1	5.1869	14.839	12.236	90.0	95.73	90.0
1.8	1	5.1893	14.832	12.199	90.0	95.76	90.0
1.91	1	5.1806	14.841	12.152	90.0	95.59	90.0
1.99	1	5.1721	14.85	12.073	90.0	95.242	90.0
2.06	1	5.1718	14.904	12.041	90.0	95.14	90.0
2.16	1	5.1626	14.916	11.963	90.0	94.79	90.0
2.36	1	5.1551	14.95	11.879	90.0	94.201	90.0
2.39	1	5.1535	14.942	11.869	90.0	94.35	90.0

Principal axis strain calculation output									
			Direction			**Empirical parameters**			
Axes	***K*** **(TPa^{-1})**	**σ*K*(TPa^{-1})**	***a***	***b***	***c***	ε_0	***λ***	p_c	***v***
X_1	52.1402	1.8325	-0.404	-0.0	0.9147	-0.0	-0.0494	1.36	1.1629
X_2	0.7752	1.9348	0.9929	0.0	0.1188	2.6275	-2.6292	1.3425	0.0002
X_3	-11.2915	1.6455	-0.0	1.0	-0.0	-0.0001	0.0101	1.36	1.5651
V	40.6353	0.7868							

Table S14. Principal axis strain calculation details for IZIYOI hp.[40] -*continuation*

Birch-Murnaghan coefficients							
	B_0 (GPa)	σB_0 (GPa)	V_0 (Å^3)	σV_0 (Å^3)	B'	$\sigma B'$	p_c (GPa)
2nd	16.6013	0.77	1021.6624	3.8216	4.0	n/a	0.0
3rd	21.831	8.8713	1009.829	17.3511	1.4355	3.8919	0.0
3rd with P_c	23.4368	2.9822	951.0629	1.2425	0.9148	4.9818	1.36

Compressibility						
p (GPa)	K_1 (TPa^{-1})	K_2 (TPa^{-1})	K_3 (TPa^{-1})	σK_1 (TPa^{-1})	σK_2 (TPa^{-1})	σK_3 (TPa^{-1})
1.36	1.1611	25.092	-0.0	447796520.0008	233.0249	9444309.5287
1.51	42.1938	2.6257	-5.4187	6.9021	5.9519	2.4897
1.65	46.9775	1.4305	-7.8647	4.6939	1.3173	2.7166
1.73	48.8794	1.1352	-9.0254	3.5419	1.3203	2.5454
1.8	50.2788	0.9616	-9.9538	2.6877	1.609	2.239
1.91	52.1402	0.7752	-11.2915	1.8325	1.9348	1.6455
1.99	53.3065	0.6795	-12.1922	1.8102	2.0686	1.3403
2.06	54.2294	0.6132	-12.9401	2.1692	2.1381	1.3859
2.16	55.422	0.5382	-13.9543	2.9538	2.1873	2.0067
2.36	57.4737	0.4324	-15.8296	4.6976	2.1887	4.0715
2.39	57.7511	0.42	-16.0962	4.9548	2.1826	4.4191
1.36	1.1611	25.092	-0.0	447796520.0008	233.0249	9444309.5287

Table S15. Principal axis strain calculation details for SULBAC. [30]

Input data							
p **(GPa)**	***σp*** **(GPa)**	***a*** **(Å)**	***b*** **(Å)**	***c*** **(Å)**	***α*** **(º)**	***β*** **(º)**	***γ*** **(º)**
0.91	1	13.4289	13.4289	13.551	90.0	90.0	90.0
1.37	1	13.2089	13.2089	13.5581	90.0	90.0	90.0
1.77	1	13.0469	13.0469	13.5793	90.0	90.0	90.0
2.04	1	12.9516	12.9516	13.5965	90.0	90.0	90.0
2.41	1	12.7987	12.7987	13.6509	90.0	90.0	90.0
2.44	1	12.8099	12.8099	13.6621	90.0	90.0	90.0
2.62	1	12.7617	12.7617	13.6588	90.0	90.0	90.0
2.83	1	12.6948	12.6948	13.6644	90.0	90.0	90.0

Principal axis strain calculation output									
			Direction			**Empirical parameters**			
Axes	***K*** **(TPa^{-1})**	***σK*** **(TPa^{-1})**	***a***	***b***	***c***	ε_0	***λ***	p_c	***v***
X_1	27.4329	1.0929	1.0	0.0	-0.0	21.3118	-21.2111	-1.7402	0.0049
X_2	27.4329	1.1628	0.0	1.0	-0.0	21.3112	-21.2105	-1.7402	0.0049
X_3	-5.8586	1.0728	-0.0	0.0	1.0	-0.0004	0.0038	0.91	1.4513
V	50.4396	2.7105							

Birch-Murnaghan coefficients							
	B_0 **(GPa)**	σB_0 **(GPa)**	V_0 **(Å^3)**	σV_0 **(Å^3)**	***B'***	***σB'***	p_c **(GPa)**
2nd	11.9026	0.4783	2605.0118	11.3594	4.0	n/a	0.0
3rd	4.8001	4.5193	2724.1058	120.1665	11.1313	8.7787	0.0
3rd with P_c	12.6794	1.3138	2443.3952	5.9512	7.4621	1.9106	0.91

Compressibility						
p **(GPa)**	K_1 **(TPa^{-1})**	K_2 **(TPa^{-1})**	K_3 **(TPa^{-1})**	σK_1 **(TPa^{-1})**	σK_2 **(TPa^{-1})**	σK_3 **(TPa^{-1})**
0.91	39.0624	39.0622	-0.0	5.9379	6.5249	1627083954.7939
1.37	33.3109	33.3109	-3.9051	1.2894	1.3561	2.6836
1.77	29.5323	29.5323	-5.1793	1.5166	1.6909	1.8083
2.04	27.4329	27.4329	-5.8586	1.0929	1.1628	1.0728
2.41	24.9985	24.9985	-6.6575	1.2628	1.3338	1.6657
2.44	24.8199	24.82	-6.7173	1.3626	1.454	1.7829
2.62	23.8002	23.8003	-7.0631	2.09	2.3139	2.5518
2.83	22.7118	22.7118	-7.4422	3.0794	3.4623	3.5196

Table S16. Principal axis strain calculation details for POWSID.[32]

Input data							
p **(GPa)**	**σ*p* (GPa)**	***a*** **(Å)**	***b*** **(Å)**	***c*** **(Å)**	***α*** **(º)**	***β*** **(º)**	***γ*** **(º)**
0.0001	1	13.3756	8.6951	16.3247	90.0	104.261	90.0
0.2	1	13.44	8.548	16.2728	90.0	103.8	90.0
0.3	1	13.511	8.349	16.23	90.0	103.663	90.0
0.48	1	13.585	8.236	16.306	90.0	103.3	90.0
0.85	1	13.59	8.07	16.21	90.0	103.33	90.0
1.82	1	13.614	7.741	16.059	90.0	102.55	90.0
2.48	1	13.562	7.541	15.878	90.0	101.57	90.0

Principal axis strain calculation output									
			Direction			**Empirical parameters**			
Axes	***K*** **(TPa^{-1})**	**σ*K*(TPa^{-1})**	***a***	***b***	***c***	ε_0	***λ***	p_c	***v***
X_1	77.6169	12.336	0.0	1.0	-0.0	0.2243	-0.2906	-0.2995	0.2199
X_2	6.7262	0.3145	-0.3518	-0.0	0.9361	0.005	-0.0	-107.8934	74.6563
X_3	-16.4071	3.5153	0.9213	0.0	0.3889	-47.0636	47.0859	-0.0872	0.0002
V	52.2003	2.0625							

Birch-Murnaghan coefficients							
	B_0 **(GPa)**	σB_0 **(GPa)**	V_0 **(Å^3)**	σV_0 **(Å^3)**	***B'***	***σB'***	p_c **(GPa)**
2nd	13.262	0.6301	1834.9542	6.3165	4.0	n/a	0.0
3rd	13.0267	2.5573	1835.5423	9.5155	4.2254	2.3825	0.0

Compressibility						
p **(GPa)**	K_1 **(TPa^{-1})**	K_2 **(TPa^{-1})**	K_3 **(TPa^{-1})**	σK_1 **(TPa^{-1})**	σK_2 **(TPa^{-1})**	σK_3 **(TPa^{-1})**
0.0001	163.6414	4.8507	-106.5924	90.1611	0.2268	107.2128
0.2	109.8316	5.5593	-32.4002	14.331	0.2599	9.1837
0.3	95.2587	5.9511	-24.0331	13.3055	0.2782	6.5576
0.48	77.6169	6.7262	-16.4071	12.336	0.3145	3.5153
0.85	57.3276	8.6457	-9.9304	6.5367	0.4042	1.9627
1.82	35.5696	16.6293	-4.8804	6.8447	0.7775	2.5094
2.48	28.7897	25.8661	-3.6259	9.9656	1.2093	2.5173

Table S17. Principal axis strain calculation details for JOHGIX ($(C_6F_5Au)_2$(μ-1,4-diisocyanobenzene)).[28]

Input data							
p **(GPa)**	***σp*** **(GPa)**	***a*** **(Å)**	***b*** **(Å)**	***c*** **(Å)**	***α*** **(º)**	***β*** **(º)**	***γ*** **(º)**
0.0001	1	5.458	9.754	18.838	90.0	91.632	90.0
0.28	1	5.5274	9.4838	18.41	90.0	92.32	90.0
0.73	1	5.5924	9.2665	17.985	90.0	92.91	90.0
1.38	1	5.6422	9.0462	17.618	90.0	93.39	90.0
2.42	1	5.6829	8.7611	17.176	90.0	94.06	90.0

Principal axis strain calculation output									
			Direction			**Empirical parameters**			
Axes	***K*** **(TPa^{-1})**	***σK*** **(TPa^{-1})**	***a***	***b***	***c***	ε_0	***λ***	p_c	***v***
X_1	43.1152	0.5159	0.0	1.0	0.0	-0.0	-0.0619	0.0001	0.618
X_2	41.8096	1.4847	0.5004	-0.0	0.8658	0.0588	-0.1107	-0.1651	0.3516
X_3	-18.7636	2.4261	0.9992	0.0	-0.0404	-64.0328	64.0589	-0.2353	0.0003
V	58.3481	5.6138							

Birch-Murnaghan coefficients							
	B_0 **(GPa)**	σB_0 **(GPa)**	V_0 **(Å^3)**	σV_0 **(Å^3)**	***B'***	***σB'***	p_c **(GPa)**
2nd	11.5677	0.8577	991.5983	6.1046	4.0	n/a	0.0
3rd	7.6442	1.4803	999.0525	5.8583	9.631	2.6898	0.0

Compressibility						
p **(GPa)**	K_1 **(TPa^{-1})**	K_2 **(TPa^{-1})**	K_3 **(TPa^{-1})**	σK_1 **(TPa^{-1})**	σK_2 **(TPa^{-1})**	σK_3 **(TPa^{-1})**
0.0001	1489144800.3671	125.0652	-76.9085	$1.67*10^{24}$	23.9058	37.3112
0.28	62.1816	65.7691	-35.1427	2.0985	2.6017	3.4775
0.73	43.1152	41.8096	-18.7636	0.5159	1.4847	2.4261
1.38	33.8035	29.3454	-11.2148	0.3377	0.7358	0.6155
2.42	27.2747	21.0184	-6.8233	0.5925	1.5078	1.3118

Table S18. Principal axis strain calculation details for MAGVOG I ([Ag(en)]NO_3-I).[25]

Input data							
p **(GPa)**	**σ*p*** **(GPa)**	***a*** **(Å)**	***b*** **(Å)**	***c*** **(Å)**	***α*** **(º)**	***β*** **(º)**	***γ*** **(º)**
0.0001	2.0	10.4305	10.5272	6.2956	90.0	115.16	90.0
0.12	1.0	10.451	10.51	6.268	90.0	115.08	90.0
0.41	1.0	10.521	10.426	6.202	90.0	115.0	90.0
0.6	1.0	10.574	10.345	6.166	90.0	114.85	90.0
0.74	1.0	10.596	10.295	6.141	90.0	114.67	90.0
0.92	1.0	10.632	10.219	6.115	90.0	114.46	90.0

Principal axis strain calculation output									
			Direction			**Empirical parameters**			
Axes	***K*** **(TPa^{-1})**	**σ*K*(TPa^{-1})**	***a***	***b***	***c***	ε_0	***λ***	p_c	***v***
X_1	32.9122	3.5933	0.0983	0.0	0.9952	26.0501	-26.0555	-0.8651	0.0016
X_2	33.5475	1.2502	-0.0	1.0	-0.0	0.0004	-0.0337	0.0001	1.3066
X_3	-28.2978	2.1506	0.9066	0.0	0.422	-0.4871	0.0877	-11.8083	0.694
V	37.2247	0.4634							

Birch-Murnaghan coefficients							
	B_0 **(GPa)**	σB_0 **(GPa)**	V_0 **(Å^3)**	σV_0 **(Å^3)**	***B'***	***σB'***	p_c **(GPa)**
2nd	24.3308	0.371	626.5322	0.2193	4.0	n/a	0.0
3rd	26.038	1.2732	626.2721	0.2567	0.583	2.3618	0.0

Compressibility						
p **(GPa)**	K_1 **(TPa^{-1})**	K_2 **(TPa^{-1})**	K_3 **(TPa^{-1})**	σK_1 **(TPa^{-1})**	σK_2 **(TPa^{-1})**	σK_3 **(TPa^{-1})**
0.0001	48.4739	0.0001	-28.5948	11.9061	7402363345627.261	9.3392
0.12	42.5831	23.0126	-28.5065	2.1993	2.7243	4.6603
0.41	32.9122	33.5475	-28.2978	3.5933	1.2502	2.1506
0.6	28.6505	37.7031	-28.1645	0.8549	1.1361	2.0364
0.74	26.1555	40.2077	-28.068	3.565	1.8237	1.8189
0.92	23.5221	42.9839	-27.946	7.7735	2.8903	5.9064

Table S19. Principal axis strain calculation details for UNIRUF II (lithium L-tartrate II). [26]

Input data							
p **(GPa)**	**σ*p*** **(GPa)**	***a*** **(Å)**	***b*** **(Å)**	***c*** **(Å)**	***α*** **(º)**	***β*** **(º)**	***γ*** **(º)**
2.01	1.0	14.67	4.946	10.365	90.0	131.97	90.0
2.29	1.0	14.639	4.9393	10.379	90.0	132.027	90.0
2.95	1.0	14.477	4.9154	10.425	90.0	132.46	90.0
3.43	1.0	14.342	4.8946	10.487	90.0	133.01	90.0
4.03	1.0	14.231	4.856	10.642	90.0	134.235	90.0
4.41	1.0	14.168	4.8351	10.715	90.0	134.825	90.0
4.66	1.0	14.126	4.8218	10.753	90.0	135.162	90.0
4.82	1.0	14.095	4.8107	10.788	90.0	135.458	90.0
5.52	1.0	14.024	4.789	10.837	90.0	135.927	90.0

Principal axis strain calculation output									
			Direction			**Empirical parameters**			
Axes	***K*** **(TPa^{-1})**	**σ*K*(TPa^{-1})**	***a***	***b***	***c***	ε_0	***λ***	p_c	***v***
X_1	35.7141	2.4393	0.7554	-0.0	0.6552	0.0036	-0.0326	2.01	1.0535
X_2	10.3729	0.5793	-0.0	1.0	-0.0	0.0006	-0.0084	2.01	1.1298
X_3	-15.3463	1.4685	0.0668	-0.0	0.9978	-0.0015	0.0119	2.01	1.157
V	29.1418	0.9977							

Birch-Murnaghan coefficients							
	B_0 **(GPa)**	σB_0 **(GPa)**	V_0 **(Å^3)**	σV_0 **(Å^3)**	***B'***	***σB'***	p_c **(GPa)**
2nd	18.8557	1.1036	615.5756	4.289	4.0	n/a	0.0
3rd	27.4966	7.7217	601.8454	10.0491	1.831	1.6631	0.0
3rd with P_c	30.7033	4.0963	561.7441	1.7144	1.3565	2.0553	2.01

Compressibility						
p **(GPa)**	K_1 **(TPa^{-1})**	K_2 **(TPa^{-1})**	K_3 **(TPa^{-1})**	σK_1 **(TPa^{-1})**	σK_2 **(TPa^{-1})**	σK_3 **(TPa^{-1})**
2.01	5.1924	0.0963	-0.1024	$382*10^{12}$	$10*10^{12}$	$0.381*10^{12}$
2.29	32.1321	8.0261	-11.253	10.1794	2.0783	4.9618
2.95	34.2823	9.3924	-13.6096	4.4526	1.1051	2.8384
3.43	35.0472	9.909	-14.5202	2.4536	0.6354	1.6622
4.03	35.7141	10.3729	-15.3463	2.4393	0.5793	1.4685
4.41	36.0449	10.6076	-15.7672	3.2611	0.7843	1.993
4.66	36.2364	10.7449	-16.0145	3.8572	0.9437	2.4131
4.82	36.3502	10.8269	-16.1625	4.2365	1.0475	2.689
5.52	36.7853	11.1441	-16.7369	5.7949	1.4869	3.8705

Table S20. Principal axis strain calculation details for $Ag_3[Co(CN)_6]$ I.[24]

Input data							
p **(GPa)**	**σ*p*** **(GPa)**	***a*** **(Å)**	***b*** **(Å)**	***c*** **(Å)**	***α*** **(º)**	***β*** **(º)**	***γ*** **(º)**
0.0001	1	7.0309	7.0309	7.1172	90.0	90.0	90.0
0.06	1	6.9913	6.9913	7.14	90.0	90.0	90.0

0.157	1	6.9065	6.9065	7.2006	90.0	90.0	90.0

Principal axis strain calculation output

			Direction			Empirical parameters			
Axes	***K*** **(TPa^{-1})**	**σ*K*(TPa^{-1})**	***a***	***b***	***c***	ε_0	λ	p_c	***v***
X_1	112.525	nan	1.0	0.0	-0.0	0.0	-0.1639	-0.0003	1.1982
X_2	112.525	nan	0.0	1.0	-0.0	0.0	-0.1639	-0.0003	1.1982
X_3	-71.656	nan	-0.0	-0.0	1.0	-0.0	0.1401	0.0	1.3431
V	152.4697	2.9733							

Birch-Murnaghan coefficients

	B_0 **(GPa)**	σB_0 **(GPa)**	V_0 **(Å^3)**	σV_0 **(Å^3)**	***B'***	***σB'***	p_c **(GPa)**
2nd	6.124	0.4014	352.0508	0.3487	4.0	n/a	0.0
3rd	7.8138	inf	351.833	inf	-12.8464	inf	0.0

Compressibility

p **(GPa)**	K_1 **(TPa^{-1})**	K_2 **(TPa^{-1})**	K_3 **(TPa^{-1})**	σK_1 **(TPa^{-1})**	σK_2 **(TPa^{-1})**	σK_3 **(TPa^{-1})**
0.0001	41.36	41.36	-6.4507	nan	nan	nan
0.06	112.525	112.525	-71.656	nan	nan	nan
0.157	136.0837	136.0837	-99.6889	nan	nan	nan

Comments

At least as many data points as parameters are needed for a fit to be carried out (e.g. 3 for 3rd order Birch-Murnaghan, 4 for empirical pressure fitting). As PASCal calculates errors from derivatives, more data points than parameters are needed for error estimates.

Table S21. Principal axis strain calculation details for $Ag_3[Co(CN)_6]$ II.[24]

Input data							
p **(GPa)**	***σp*** **(GPa)**	***a*** **(Å)**	***b*** **(Å)**	***c*** **(Å)**	***α*** **(º)**	***β*** **(º)**	***γ*** **(º)**
0.19	1.0	6.6985	11.5782	6.5554	90.0	78.522	90.0
0.226	1.0	6.6934	11.5391	6.5661	90.0	78.521	90.0
0.29	2.0	6.68	11.468	6.577	90.0	78.47	90.0
0.294	1.0	6.6745	11.497	6.5707	90.0	78.473	90.0
0.395	1.0	6.6415	11.4251	6.5959	90.0	78.284	90.0
0.55	2.0	6.605	11.295	6.629	90.0	78.21	90.0
0.78	2.0	6.553	11.196	6.646	90.0	77.967	90.0
0.9	2.0	6.539	11.156	6.654	90.0	77.871	90.0
0.92	2.0	6.5333	11.154	6.6507	90.0	77.91	90.0
1.08	2.0	6.505	11.116	6.663	90.0	77.73	90.0
1.87	2.0	6.4172	10.922	6.696	90.0	77.584	90.0
3.02	2.0	6.2904	10.739	6.747	90.0	77.39	90.0
5.13	2.0	6.0657	10.493	6.833	90.0	77.09	90.0
6.92	2.0	5.91	10.333	6.891	90.0	77.01	90.0
7.65	2.0	5.8657	10.27	6.908	90.0	76.921	90.0

Principal axis strain calculation output									
			Direction			**Empirical parameters**			
Axes	***K*** **(TPa^{-1})**	**σ*K*(TPa^{-1})**	***a***	***b***	***c***	ε_0	***λ***	p_c	***v***
X_1	31.7957	1.008	0.0	1.0	0.0	0.0782	-0.1162	-0.0215	0.2575
X_2	27.49	0.9349	0.9718	0.0	-0.236	0.0061	-0.0376	0.1383	0.6671
X_3	-11.906	0.6378	0.0397	0.0	0.9992	-0.004	0.0206	0.1561	0.4994
V	25.2773	1.4075							

Birch-Murnaghan coefficients							
	B_0 **(GPa)**	σB_0 **(GPa)**	V_0 **(Å^3)**	σV_0 **(Å^3)**	***B'***	***σB'***	p_c **(GPa)**
2nd	23.2904	0.8843	498.2556	1.5382	4.0	n/a	0.0
3rd	10.741	1.3371	505.3077	1.6002	13.2503	1.808	0.0
3rd with P_c	13.1187	1.0592	497.3116	0.8894	11.8886	1.2382	0.19

Table S21. Principal axis strain calculation details for $Ag_3[Co(CN)_6]$ II. ^{24}- *continuation*

Compressibility						
p **(GPa)**	K_1 **(TPa^{-1})**	K_2 **(TPa^{-1})**	K_3 **(TPa^{-1})**	σK_1 **(TPa^{-1})**	σK_2 **(TPa^{-1})**	σK_3 **(TPa^{-1})**
0.19	94.8203	67.2893	-55.8581	12.3528	25.1915	32.8753
0.226	84.3772	56.4415	-38.8899	7.9521	9.9985	7.9964
0.29	71.1337	47.0339	-28.0899	3.9257	3.4292	2.2128
0.294	70.463	46.6283	-27.6791	3.7678	3.2571	2.1208
0.395	57.3346	39.481	-21.0231	1.6294	1.5211	1.4045
0.55	45.3323	33.7372	-16.3678	1.2027	1.2457	1.0921
0.78	35.2658	29.1042	-13.002	1.103	1.0406	0.7612
0.9	31.7957	27.49	-11.906	1.008	0.9349	0.6378
0.92	31.2928	27.2539	-11.7489	0.9911	0.918	0.6198
1.08	27.8507	25.616	-10.6821	0.8551	0.7915	0.4967
1.87	18.642	20.9148	-7.84	0.3773	0.3819	0.2096
3.02	13.1019	17.6537	-6.0631	0.2327	0.2295	0.1899
5.13	8.8598	14.7033	-4.5992	0.3598	0.3988	0.2694
6.92	7.1	13.2775	-3.9433	0.4116	0.5099	0.3031
7.65	6.592	12.8333	-3.746	0.4227	0.5437	0.3117
Comments						
For input data σp=2 set for neutron powder data.						

Table S22. Principal axis strain calculation details for $Zn[Au(CN)_2]_2$ I.[29]

Input data							
p **(GPa)**	***σp*** **(GPa)**	***a*** **(Å)**	***b*** **(Å)**	***c*** **(Å)**	***α*** **(º)**	***β*** **(º)**	***γ*** **(º)**
0.35	1.0	8.2549	8.2549	21.1181	90.0	90.0	90.0
0.79	2.0	8.0921	8.0921	21.438	90.0	90.0	90.0
0.95	1.0	8.0278	8.0278	21.6073	90.0	90.0	90.0
1.02	2.0	8.0051	8.0051	21.612	90.0	90.0	90.0
1.17	2.0	7.949	7.949	21.7	90.0	90.0	90.0
1.3	1.0	7.8537	7.8537	21.9417	90.0	90.0	90.0
1.36	2.0	7.793	7.793	22.048	90.0	90.0	90.0
1.5	1.0	7.8066	7.8066	22.0406	90.0	90.0	90.0
1.56	2.0	7.7208	7.7208	22.147	90.0	90.0	90.0
1.78	1.0	7.6743	7.6743	22.2592	90.0	90.0	90.0

Principal axis strain calculation output									
			Direction			**Empirical parameters**			
Axes	***K*** **(TPa^{-1})**	***σK*** **(TPa^{-1})**	***a***	***b***	***c***	ε_0	***λ***	p_c	***v***
X_1	53.1254	4.7515	1.0	0.0	-0.0	0.0003	-0.0504	0.35	1.0687
X_2	53.1254	4.7515	0.0	1.0	-0.0	0.0003	-0.0504	0.35	1.0687
X_3	-37.0697	4.2737	-0.0	-0.0	1.0	-12.7036	12.0285	-7.7778	0.026
V	64.0214	2.2508							

Birch-Murnaghan coefficients							
	B_0 **(GPa)**	σB_0 **(GPa)**	V_0 **(Å^3)**	σV_0 **(Å^3)**	***B'***	***σB'***	p_c **(GPa)**
2nd	10.6608	0.8634	1495.3125	10.0139	4.0	n/a	0.0
3rd	18.2885	2.1614	1468.4336	6.2722	-1.5656	1.2311	0.0
3rd with P_c	17.6345	1.715	1440.1221	3.5827	-2.1964	1.4451	0.35

Table S22. Principal axis strain calculation details for $Zn[Au(CN)_2]_2$ I.[29]- *continuation*

Compressibility						
p **(GPa)**	K_1 **(TPa^{-1})**	K_2 **(TPa^{-1})**	K_3 **(TPa^{-1})**	σK_1 **(TPa^{-1})**	σK_2 **(TPa^{-1})**	σK_3 **(TPa^{-1})**
0.35	4.1105	4.1105	-40.7076	$2.86*10^{15}$	$2.86*10^{15}$	14.773
0.79	50.9001	50.9001	-38.6701	16.0506	16.0506	3.2399
0.95	51.9968	51.9968	-37.9795	10.3785	10.3785	4.425
1.02	52.3927	52.3927	-37.6852	8.3	8.3	4.6268
1.17	53.1254	53.1254	-37.0697	4.7515	4.7515	4.2737
1.3	53.6654	53.6654	-36.5526	3.4508	3.4508	3.3753
1.36	53.8918	53.8918	-36.3188	3.7184	3.7184	3.0259
1.5	54.3748	54.3748	-35.7849	5.5891	5.5891	3.7155
1.56	54.5652	54.5652	-35.561	6.5775	6.5775	4.7959
1.78	55.1954	55.1954	-34.7635	10.2397	10.2397	10.9939
Comments						
For input data σ*p*=2 set for powder data. The lower limit not equal 0.1 MPa does not mean the NLC is not present starting from ambient conditions, but the compressibility value lack a physical sense.						

Compressibility reported in original paper [29]		
p **(GPa)**	K_a **(TPa^{-1})**	K_c **(TPa^{-1})**
0.35	55(16)	−48(14)
0.79	53(5)	−44(4)
0.95	53(4)	−43.6(29)
1.02	53(3)	−43.3(29)
1.17	53(4)	−43(3)
1.3	53(5)	−42(4)
1.36	52(6)	−42(5)
1.47	52(6)	−42(5)
1.5	52(7)	−42(5)
1.56	52(7)	−42(6)
1.78	52(9)	−41(7)

Table S23. Principal axis strain calculation details for $Zn[Au(CN)_2]_2$ II.[29]

Input data							
p **(GPa)**	**σ*p* (GPa)**	***a*** **(Å)**	***b*** **(Å)**	***c*** **(Å)**	***α*** **(º)**	***β*** **(º)**	***γ*** **(º)**
2.04	1	15.227	15.227	44.64	90.0	90.0	90.0
2.23	1	15.165	15.165	44.75	90.0	90.0	90.0
2.37	1	15.101	15.101	44.85	90.0	90.0	90.0
3.46	1	14.71	14.71	45.27	90.0	90.0	90.0
3.88	1	14.57	14.57	45.43	90.0	90.0	90.0
4.69	1	14.452	14.452	45.66	90.0	90.0	90.0
6.13	1	14.117	14.117	45.67	90.0	90.0	90.0
7.62	1	14.005	14.005	46.19	90.0	90.0	90.0
10.66	1	13.73	13.73	46.2	90.0	90.0	90.0
14.22	1	13.342	13.342	45.93	90.0	90.0	90.0

Principal axis strain calculation output									
			Direction			**Empirical parameters**			
Axes	***K*** **(TPa^{-1})**	**σ*K*(TPa^{-1})**	***a***	***b***	***c***	ε_0	***λ***	p_c	***v***
X_1	16.1133	1.2338	0.0	1.0	-0.0	0.0833	-0.0936	1.3862	0.3204
X_2	16.1133	1.2338	1.0	0.0	-0.0	0.0833	-0.0936	1.3862	0.3204
X_3	-4.4942	0.9505	-0.0	-0.0	1.0	-79.7413	79.7518	1.7485	0.0001
V	16.7411	1.2388							

Birch-Murnaghan coefficients							
	B_0 **(GPa)**	σB_0 **(GPa)**	V_0 **(Å^3)**	σV_0 **(Å^3)**	***B'***	***σB'***	p_c **(GPa)**
2nd	27.2682	2.3456	10932.6306	129.011	4.0	n/a	0.0
3rd	16.0205	12.1261	11314.2102	592.4585	6.5229	3.7073	0.0
3rd with P_c	28.2314	6.9697	10299.1811	114.1907	5.617	1.9951	2.04

Table S23. Principal axis strain calculation details for $Zn[Au(CN)_2]_2$ II.[29]- *continuation*

Compressibility						
p **(GPa)**	K_1 **(TPa^{-1})**	K_2 **(TPa^{-1})**	K_3 **(TPa^{-1})**	σK_1 **(TPa^{-1})**	σK_2 **(TPa^{-1})**	σK_3 **(TPa^{-1})**
2.04	40.0247	40.0247	-32.8527	16.2519	16.2519	43.2239
2.23	33.6533	33.6533	-19.8907	7.7344	7.7344	10.2256
2.37	30.3193	30.3193	-15.4107	4.6499	4.6499	4.5118
3.46	18.2649	18.2649	-5.5969	1.2997	1.2997	1.1827
3.88	16.1133	16.1133	-4.4942	1.2338	1.2338	0.9505
4.69	13.3097	13.3097	-3.2568	0.9579	0.9579	0.6623
6.13	10.4086	10.4086	-2.1865	0.5249	0.5249	0.4609
7.62	8.6452	8.6452	-1.6317	0.3683	0.3683	0.406
10.66	6.5999	6.5999	-1.0751	0.5677	0.5677	0.3762
14.22	5.2924	5.2924	-0.7683	0.7701	0.7701	0.3517

Compressibility reported in original paper [29]		
p **(GPa)**	K_a **(TPa^{-1})**	K_c **(TPa^{-1})**
2.04	75(5)	−51(3)
2.2	51(5)	−31(3)
2.2335	48(5)	−30(3)
2.368	39(5)	−23(3)
2.4	38(5)	−21(3)
3.1	22(5)	−10(3)
3.4575	18(5)	−8(3)
3.6	18(5)	−7(3)
3.8755	16(5)	−6(3)
4.6905	13(5)	−4(3)
4.89	13(5)	−3(3)
6.128	10(5)	−2(3)
7.1	9(5)	−1(3)
7.6165	8(5)	−1(3)
9.54	7(5)	0(3)
10.66	6(5)	0(3)
12	6(5)	0(3)
14.223	5(5)	0(3)

Table S24. Principal axis strain calculation details for LOCCAI.[37]

Input data							
p **(GPa)**	**σ*p* (GPa)**	***a*** **(Å)**	***b*** **(Å)**	***c*** **(Å)**	***α*** **(º)**	***β*** **(º)**	***γ*** **(º)**
0.12	1	13.47	8.649	13.025	90.0	109.3	90.0
0.19	1	13.491	8.626	12.8826	90.0	109.63	90.0
0.23	1	13.52	8.6272	12.882	90.0	110.29	90.0
0.34	1	13.522	8.6312	12.88	90.0	110.04	90.0

Principal axis strain calculation output									
			Direction			**Empirical parameters**			
Axes	***K*** **(TPa^{-1})**	**σ*K*(TPa^{-1})**	***a***	***b***	***c***	ε_0	***λ***	p_c	***v***
X_1	34.6693	nan	0.3398	-0.0	0.9405	8.2668	-8.288	0.1198	0.0003
X_2	1.9224	nan	0.0	1.0	-0.0	0.1518	-0.1545	0.12	0.0009
X_3	-24.8607	nan	0.9987	0.0	-0.0508	-5.3334	5.342	0.0884	0.0005
V	55.472	28.2567							

Birch-Murnaghan coefficients							
	B_0 **(GPa)**	σB_0 **(GPa)**	V_0 **(Å^3)**	σV_0 **(Å^3)**	***B'***	***σB'***	p_c **(GPa)**
2nd	7.801	6.4171	1454.6702	31.2922	4.0	n/a	0.0
3rd	46.4834	67.2252	1436.32	7.8691	-74.858	60.2275	0.0
3rd with P_c	36.293	60.2917	1432.1634	4.1382	-97.8947	56.4451	0.12

Compressibility						
p **(GPa)**	K_1 **(TPa^{-1})**	K_2 **(TPa^{-1})**	K_3 **(TPa^{-1})**	σK_1 **(TPa^{-1})**	σK_2 **(TPa^{-1})**	σK_3 **(TPa^{-1})**
0.12	15061.4126	88758178.6212	-79.9052	nan	nan	nan
0.19	34.6693	1.9224	-24.8607	nan	nan	nan
0.23	22.0837	1.2238	-17.8402	nan	nan	nan
0.34	11.0522	0.6123	-10.0429	nan	nan	nan

Table S25. Principal axis strain calculation details for LUKWAS/LUKWOG (BTCP·dItFB). [27]

Input data							
p **(GPa)**	***σp*** **(GPa)**	***a*** **(Å)**	***b*** **(Å)**	***c*** **(Å)**	***α*** **(º)**	***β*** **(º)**	***γ*** **(º)**
0.0001	1.0	17.2451	27. 2415	7.9554	90.0	90.0	90.0
0.4	1.0	17.475	26.52	7.662	90.0	90.0	90.0
0.7	1.0	17.449	26.511	7.536	90.0	90.0	90.0
1.09	1.0	17.559	26.315	7.259	90.0	90.0	90.0
1.59	1.0	17.604	25.83	7.13	90.0	90.0	90.0
1.95	1.0	17.564	25.64	7.07	90.0	90.0	90.0
2.5	1.0	17.606	25.58	6.944	90.0	90.0	90.0

Principal axis strain calculation output									
			Direction			**Empirical parameters**			
Axes	***K*** **(TPa^{-1})**	***σK*** **(TPa^{-1})**	***a***	***b***	***c***	ε_0	***λ***	p_c	***v***
X_1	51.2214	5.0105	-0.0	0.0	1.0	135.4479	-135.4741	-0.7464	0.0007
X_2	21.7061	3.6015	-0.0	1.0	-0.0	-0.0004	-0.0375	0.0001	0.5984
X_3	-4.4524	1.4573	1.0	0.0	-0.0	-0.0178	0.034	-0.0104	0.1422
V	64.5713	6.8323							

Birch-Murnaghan coefficients							
	B_0 **(GPa)**	σB_0 **(GPa)**	V_0 **(Å^3)**	σV_0 **(Å^3)**	***B'***	***σB'***	p_c **(GPa)**
2nd	9.8343	0.7679	3701.682	28.3932	4.0	n/a	0.0
3rd	5.431	2.424	3757.7874	57.5502	10.9431	5.5951	0.0

Compressibility						
p **(GPa)**	K_1 **(TPa^{-1})**	K_2 **(TPa^{-1})**	K_3 **(TPa^{-1})**	σK_1 **(TPa^{-1})**	σK_2 **(TPa^{-1})**	σK_3 **(TPa^{-1})**
0.0001	125.929	233331633.7819	-241.6246	52.8922	$2.21*10^{22}$	2644.8513
0.4	82.0245	32.4672	-10.3764	8.9627	22.5723	11.9302
0.7	65.0219	25.9314	-6.4807	7.9179	9.4603	3.9019
1.09	51.2214	21.7061	-4.4524	5.0105	3.6015	1.4573
1.59	40.2664	18.6521	-3.2289	5.0434	4.4674	1.966
1.95	34.8938	17.1843	-2.7131	7.2163	5.9388	2.3042
2.5	28.9858	15.5523	-2.1945	10.2558	7.5955	2.5567

Table S26. Principal axis strain calculation details for OTELEH.[41]

Input data							
p **(GPa)**	**σ*p* (GPa)**	***a*** **(Å)**	***b*** **(Å)**	***c*** **(Å)**	***α*** **(º)**	***β*** **(º)**	***γ*** **(º)**
0.000101	1	9.7872	8.4868	7.407	90.0	100.43	90.0
0.1	1	9.7823	8.4929	7.412	90.0	100.44	90.0
0.36	1	9.7272	8.4963	7.332	90.0	100.45	90.0
0.51	1	9.6758	8.4905	7.306	90.0	100.43	90.0
0.88	1	9.6118	8.4921	7.251	90.0	100.4	90.0
1.21	1	9.5551	8.501	7.182	90.0	100.35	90.0
1.63	1	9.4961	8.5028	7.127	90.0	100.38	90.0
1.94	1	9.4462	8.5075	7.057	90.0	100.46	90.0
2.46	1	9.3869	8.5115	6.98	90.0	100.5	90.0
3.08	1	9.3265	8.5118	6.889	90.0	100.68	90.0
3.6	1	9.2779	8.5031	6.835	90.0	100.76	90.0
4.06	1	9.2492	8.5144	6.769	90.0	100.94	90.0
4.54	1	9.2008	8.5014	6.745	90.0	100.94	90.0
5.0	1	9.1703	8.4987	6.695	90.0	101.01	90.0
5.52	1	9.1302	8.4972	6.657	90.0	101.0	90.0
6.0	1	9.1044	8.4959	6.628	90.0	100.98	90.0
6.52	1	9.07	8.4856	6.61	90.0	100.98	90.0

Principal axis strain calculation output									
			Direction			**Empirical parameters**			
Axes	***K*** **(TPa^{-1})**	**σ*K*(TPa^{-1})**	***a***	***b***	***c***	ε_0	λ	p_c	***v***
X_1	11.8879	0.2057	0.9971	0.0	0.0758	29.463	-29.4245	-2.0192	0.0018
X_2	19.4528	0.378	0.0941	-0.0	0.9956	142.4574	-142.3235	-3.2553	0.0008
X_3	-0.0929	0.1068	0.0	1.0	-0.0	-2.9759	2.9773	-0.0018	0.0001
V	27.6807	1.3696							

Table S26. Principal axis strain calculation details for OTELEH.[41]- *continuation*

Birch-Murnaghan coefficients							
	B_0 (GPa)	σB_0 (GPa)	V_0 (Å^3)	σV_0 (Å^3)	B'	$\sigma B'$	p_c (GPa)
2nd	22.4253	0.5695	603.0737	1.5866	4.0	n/a	0.0
3rd	15.7656	1.183	608.8599	1.7233	7.5085	0.7596	0.0

Compressibility						
p (GPa)	K_1 (TPa^{-1})	K_2 (TPa^{-1})	K_3 (TPa^{-1})	σK_1 (TPa^{-1})	σK_2 (TPa^{-1})	σK_3 (TPa^{-1})
0.0001	26.3317	34.1371	-119.1266	1.9326	3.127	1646.6524
0.1	25.0926	33.1214	-2.2453	1.527	2.7207	4.4466
0.36	22.3552	30.7412	-0.6319	0.8132	1.9077	0.8388
0.51	21.0317	29.5175	-0.4467	0.562	1.5644	0.5187
0.88	18.3521	26.8784	-0.2593	0.2783	0.9912	0.2559
1.21	16.4799	24.8935	-0.1887	0.2572	0.7023	0.1818
1.63	14.5864	22.755	-0.1401	0.2659	0.5081	0.1408
1.94	13.4463	21.3982	-0.1178	0.2527	0.4336	0.1242
2.46	11.8879	19.4528	-0.0929	0.2057	0.378	0.1068
3.08	10.4449	17.5504	-0.0742	0.1467	0.3908	0.0937
3.6	9.48	16.2202	-0.0635	0.1274	0.4516	0.0858
4.06	8.7639	15.201	-0.0563	0.1439	0.5278	0.0802
4.54	8.1237	14.2657	-0.0503	0.1808	0.6175	0.0753
5.0	7.5923	13.4714	-0.0457	0.2216	0.7062	0.0712
5.52	7.0695	12.6737	-0.0414	0.2672	0.8046	0.0673
6.0	6.6471	12.0169	-0.0381	0.3062	0.8911	0.0641
6.52	6.243	11.3782	-0.0351	0.3445	0.9789	0.061

Table S27. Principal axis strain calculation details for VOFVAN. [38]

Input data							
p **(GPa)**	**σ*p* (GPa)**	***a*** **(Å)**	***b*** **(Å)**	***c*** **(Å)**	***α*** **(º)**	***β*** **(º)**	***γ*** **(º)**
1.0	1	8.953	3.865	13.081	90.0	90.47	90.0
2.0	1	9.047	3.6626	12.7481	90.0	92.304	90.0
3.5	1	9.0625	3.5605	12.5539	90.0	92.541	90.0
6.2	1	9.0721	3.4383	12.285	90.0	92.72	90.0

Principal axis strain calculation output									
			Direction			**Empirical parameters**			
Axes	***K*** **(TPa^{-1})**	**σ*K*(TPa^{-1})**	***a***	***b***	***c***	ε_0	***λ***	p_c	***v***
X_1	25.1819	nan	0.0	1.0	-0.0	-0.0	-0.0534	1.0	0.4715
X_2	14.4966	nan	0.4874	0.0	0.8732	-0.0001	-0.0312	1.0	0.465
X_3	-0.9325	nan	0.9686	0.0	-0.2486	-0.151	0.1675	1.0	0.0056
V	27.4607	4.033							

Birch-Murnaghan coefficients							
	B_0 **(GPa)**	σB_0 **(GPa)**	V_0 **(Å^3)**	σV_0 **(Å^3)**	***B'***	***σB'***	p_c **(GPa)**
2nd	20.3478	4.2182	465.4972	10.8783	4.0	n/a	0.0
3rd	0.0227	3970.9403	513.9342	28749.7392	3124.4678	545151911.6272	0.0
3rd with P_c	8.5039	4.8936	451.4284	6.2087	23.1314	13.2673	1.0

Compressibility						
p **(GPa)**	K_1 **(TPa^{-1})**	K_2 **(TPa^{-1})**	K_3 **(TPa^{-1})**	σK_1 **(TPa^{-1})**	σK_2 **(TPa^{-1})**	σK_3 **(TPa^{-1})**
1.0	6799334161.5735	4981241947.5033	-104746332.035	nan	nan	nan
2.0	25.1819	14.4966	-0.9325	nan	nan	nan
3.5	15.5165	8.8789	-0.3749	nan	nan	nan
6.2	10.5368	6.0005	-0.181	nan	nan	nan

Table S28. Principal axis strain calculation details for YIHHON.[39]

Input data							
p **(GPa)**	**σ*p* (GPa)**	***a*** **(Å)**	***b*** **(Å)**	***c*** **(Å)**	***α*** **(º)**	***β*** **(º)**	***γ*** **(º)**
2.48	0.02	5.918	7.7502	8.2755	90.0	90.0	90.0
2.9	0.02	5.9522	7.6818	8.1087	90.0	90.0	90.0
3.35	0.02	5.9823	7.6367	7.9823	90.0	90.0	90.0
3.68	0.02	6.0049	7.5908	7.888	90.0	90.0	90.0

Principal axis strain calculation output									
			Direction			**Empirical parameters**			
Axes	***K*** **(TPa^{-1})**	**σ*K*(TPa^{-1})**	***a***	***b***	***c***	ε_0	***λ***	p_c	***v***
X_1	39.3254	nan	-0.0	-0.0	1.0	-0.0	-0.041	2.48	0.8246
X_2	16.8161	nan	-0.0	1.0	0.0	-0.0001	-0.0174	2.48	0.8461
X_3	-12.0829	nan	1.0	0.0	-0.0	0.0	0.0123	2.48	0.8915
V	43.0708	1.8044							

Birch-Murnaghan coefficients							
	B_0 **(GPa)**	σB_0 **(GPa)**	V_0 **(Å^3)**	σV_0 **(Å^3)**	***B'***	***σB'***	p_c **(GPa)**
2nd	11.296	1.0597	444.6265	5.7496	4.0	n/a	0.0
3rd	0.0442	1808.1917	546.6209	62548.3065	355.0833	14246417.6807	0.0
3rd with P_c	17.3155	4.0431	379.4074	1.0025	10.2068	9.0454	2.48

Compressibility						
p **(GPa)**	K_1 **(TPa^{-1})**	K_2 **(TPa^{-1})**	K_3 **(TPa^{-1})**	σK_1 **(TPa^{-1})**	σK_2 **(TPa^{-1})**	σK_3 **(TPa^{-1})**
2.48	16677.7332	2284.0323	-509.9918	nan	nan	nan
2.9	39.3254	16.8161	-12.0829	nan	nan	nan
3.35	34.6086	15.0335	-11.1646	nan	nan	nan
3.68	32.71	14.3077	-10.7817	nan	nan	nan

Table S29. Compressibility *K* (TPa^{-1}) for $InH(BDC)_2$ from Figure 2 of the original paper[19].

***p* (GPa)**	***K* (TPa^{-1})**
0.0001	-117.183
0.04	-97.042
0.099	-80.563
0.216	-68.357
0.323	-62.254
0.442	-57.981
0.534	-55.54

Function fitted to the *K* values: $K = -47.10638 \times (p + 0.03608)^{-0.27525}$ ($R^2 = 0.99878$).

Table S30. Compressibility *K* (TPa^{-1}) for MIL-53(Al) from Figure 2 of the original paper[20].

***p* (GPa)**	***K* (TPa^{-1})**
0.0001	-39.273
0.292	-22.909
0.901	-12.545
1.807	-7.091

Function fitted to the *K* values: $K = -40.5622 + 27.83138 \times p^{0.33953}$ ($R^2 = 0.99652$)

4. Compressibility capacity values for selected NLC materials

Table S31. Compressibility capacity values calculated for selected NLC materials.

NLC material	χ_K (%) for selected Δp (GPa)				
	0.15 GPa	0.90 GPa	2.00 GPa	3.00 GPa	Complete pressure range (given in brackets)
ETYFUM	0.52	2.595	4.721	6.152	6.846 (0.1 MPa-3.58 GPa)
CPOS-1	0.059	2.503	-	-	5.401 (1.02-2.32 GPa)
water@CPOS-1	0.057	0.712	-	-	2.113 (0.58-2.53 GPa)
BIUREA II	0.827	1.766	2.231	-	2.285 (0.62-2.81 GPa)
QAXMEH yellow	0.054	0.42	1.044	-	1.225 (0.54-2.84 GPa)
IZIYOI hp	0.052	0.858	-	-	1.059 (1.36-2.39 GPa)
SULBAC	0.024	0.328	-	-	0.984 (0.91-2.83 GPa)
POWSID	0.391	1.321	1.931	-	2.039 (0.1MPa-2.28 GPa)
JOHGIX	0.892	2.85	4.077	-	4.389 (0.1MPa-2.42 GPa)
MAGVOG I	0.428	2.544	-	-	2.544 (0.1MPa-0.9 GPa)
UNIRUF II	0.128	1.047	2.644	4.229	5.056 (2.01-5.51 GPa)
$Ag_3[Co(CN)_6]$ I	1.096	-	-	-	1.164 (0.1 MPa-0.157 GPa)-
$Ag_3[Co(CN)_6]$ II	0.512	1.617	2.56	3.208	5.251 (0.19-7.65 GPa)
$Zn[Au(CN)_2]_2$ I	0.605	3.479	-	-	5.374 (0.35-1.75 GPa)
$Zn[Au(CN)_2]_2$ II	0.4	1.352	1.978	2.325	3.602 (2.04-14.44 GPa)
$InH(DBC)_2$	1.34	-	-	-	3.72 (0.1 MPa-0.53 GPa)
MIL-53(Al)	0.45	1.85	-	-	2.74 0.1 MPa-1.8 GPa)

5. Wine rack motif geometry.

Table S32. parameters of a triangle formed by centroids acting as hinge points in structure of ETYFUM for pressure in 0.1 MPa-3.58 GPa range.

p (GPa)	d_1 (Å)	d_2 (Å)	h (Å)	φ (°)
0.0001	3.896	4.817	3.06	76.36
0.08	3.896	4.788	3.07	75.84
0.15	3.904	4.773	3.09	75.36
0.29	3.877	4.702	3.08	74.66
0.35	3.883	4.659	3.11	73.74
0.53	3.865	4.592	3.11	72.9
0.79	3.882	4.521	3.16	71.22
0.88	3.853	4.482	3.13	71.12
1.25	3.839	4.376	3.15	69.48
1.33	3.837	4.317	3.17	68.48
1.85	3.84	4.246	3.2	67.14
2.44	3.852	4.15	3.25	65.18
3	3.841	4.056	3.26	63.74
3.58	3.884	3.993	3.35	61.86

Table S33. Functions fitted to parameters of a the triangle formed by centroids acting as hinge points.

Parameter (y)	Fitted function ($y = a - bc^x$)	R^2
d_1	$d_1 = 3.8498 + 0.05528 * 0.13452^p$	0.63888
d_2	$d_2 = 3.81982 + 1.00592 * 0.6191^p$	0.99751
h	$h = 44.62773 - 41.5565 * 0.99826^p$	0.96756
φ	$\varphi = 56.70518 + 19.60681 * 0.70146^p$	0.99713

6. H-bond energy.

Table S34. Complexation energy calculated for selected aggregates of ETY and FUM. Short O-H···N hydrogen bond is shown in yellow and longer C-H···O hydrogen bond is shown in purple in the figures representing two types of ETY and FUM aggregates.

Aggregate		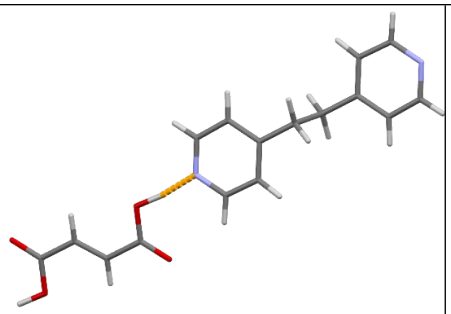	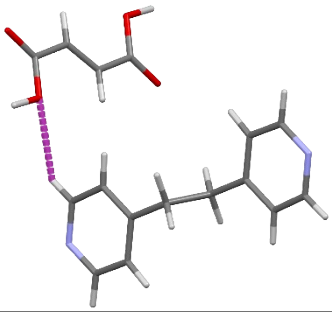
H-bond		O-H···N	C-H···O
Counterpoise corrected energy (Ha)		-1029.726279065285	-1029.701476005206
BSSE energy (Ha)		0.001869589899	0.001331073901
Sum of fragments (Ha)		-1029.702232724450	-1029.702236872457
Complexation energy (kcal/mol)	**Raw**	-16.26	-0.36
	Corrected	-15.09	0.48

Figures

1. Sample crystals

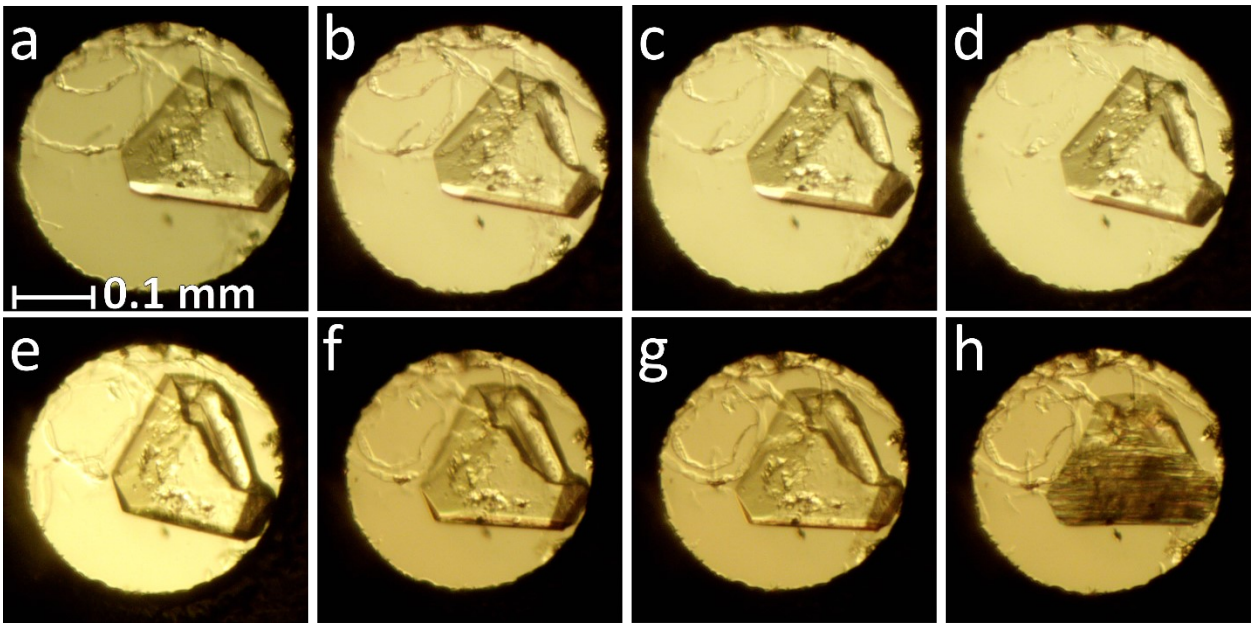

Figure S1. Sample crystal A at 298 K and (a) 3.00(2) GPa, gradually decompressed to (b) 2.44(2) GPa, (c) 1.85(2) GPa, (d) 1.25(2) GPa and (e) 0.35(2) GPa. Sample was then compressed from 0.35 GPa to (f) 2.02(2) GPa, (g) 2.06(2) GPa and (h) 3.75(2) GPa, when sample crystal was destroyed. Scale for all segments is included in lower left corner of segment (a). Cellulose fibers used to hold sample crystal in place is visible in the upper part of the chamber, while ruby chip used for pressure measurement is visible in the lower right part of the chamber next to the gasket edge.

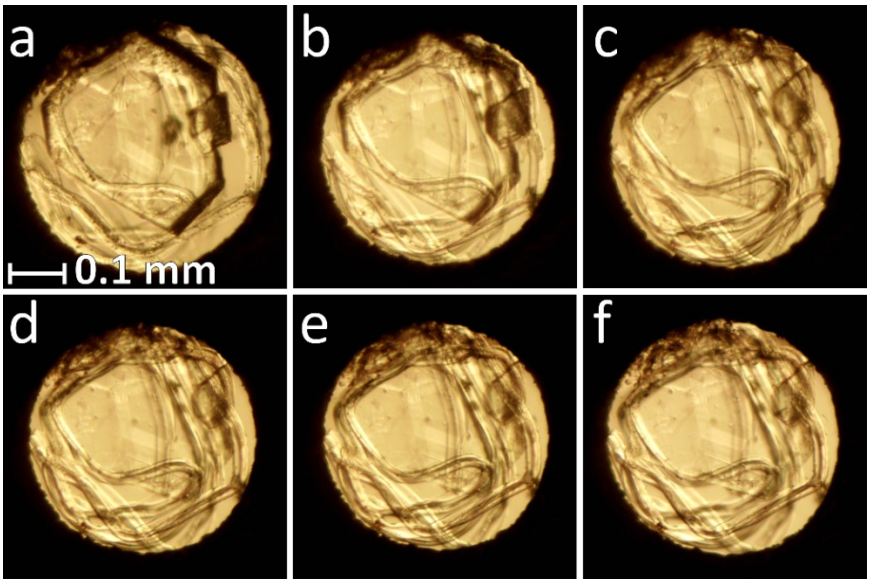

Figure S2. Sample crystal B at 298 K and (a) 0.1 MPa (just after loading sample into DAC), compressed rapidly to (f) 3.58 GPa. Pictures were taken on compression at (b) 0.64(2) GPa, (c) 1.50(2) GPa, (d) 2.49(2) GPa and (e) 3.22(2) GPa. Scale for all segments is included in lower left corner of segment (a). Cellulose fibers used to hold sample crystal in place is visible around sample crystal, while ruby chip used for pressure measurement is visible in the upper right part of the chamber next to the sample crystal.

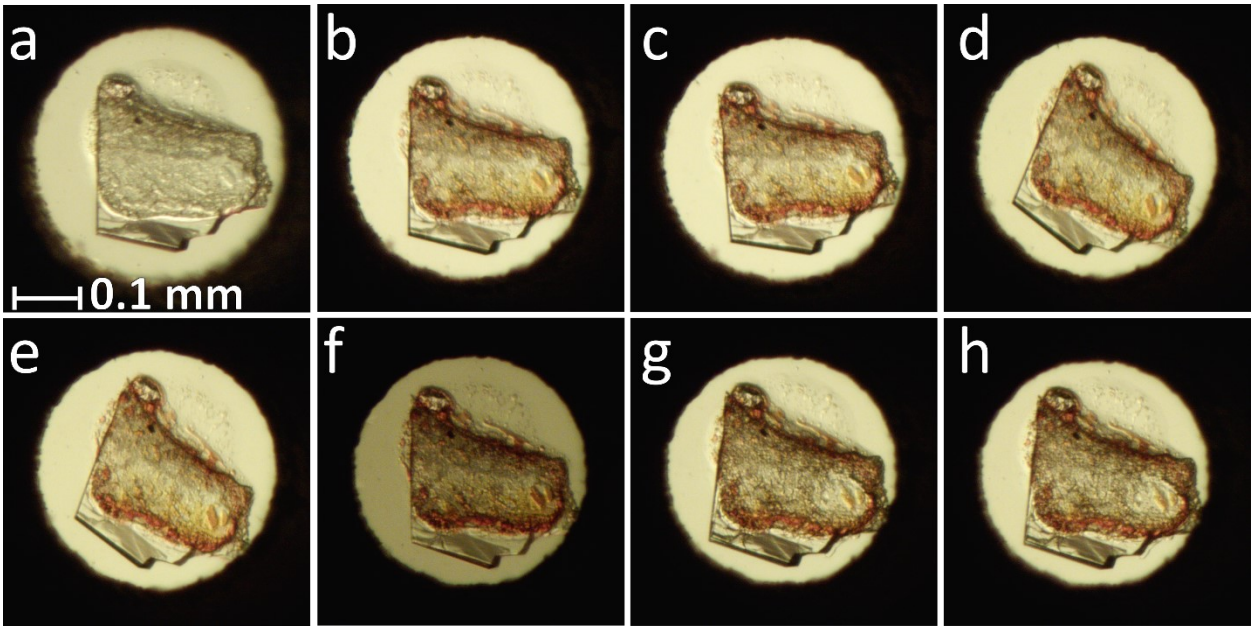

Figure S3. Sample crystal C at 298 K and at 298 K and (a) 0.1 MPa (just after loading sample into DAC), gradually compressed to (b,c) 0.29(2) GPa, (d) 0.53(2) GPa, (e) 0.88(2) GPa and (f) 1.33(2) GPa. Sample was then decompressed down to ambient pressure and compressed to (g) 0.08(2) GPa and subsequently to (h) 0.15(2) GPa. Scale for all segments is included in lower left corner of segment (a). A drop of glue used to hold sample crystal in place, and to assure its tilted position is visible "under" the sample crystal. Ruby chip used for pressure measurement is visible in the upper part of the chamber, next to the left upper corner of the sample crystal.

2. PXRD patterns

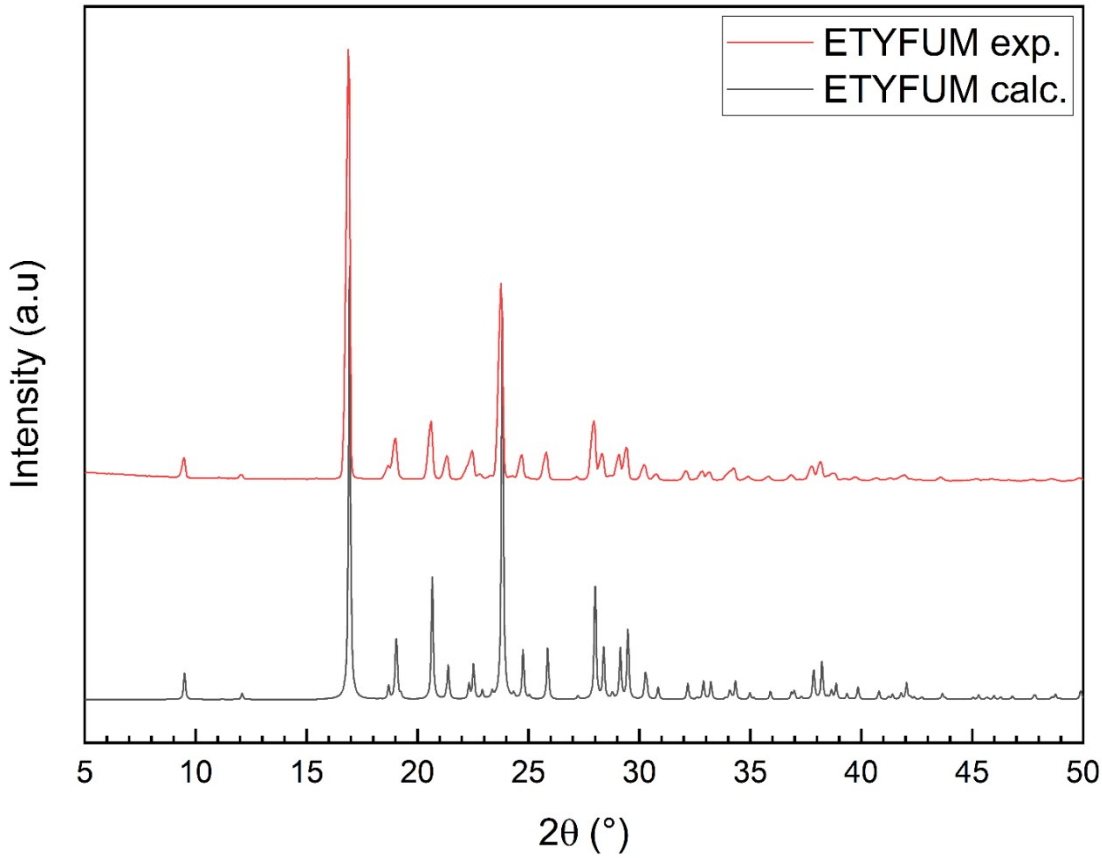

Figure S4. PXRD patterns of ETYFUM: calculated based on crystal structure (black) and experimental pattern measured for powder sample of ETYFUM received after solvent-assisted ball milling (red).

3. Principal axis strain of ETYFUM

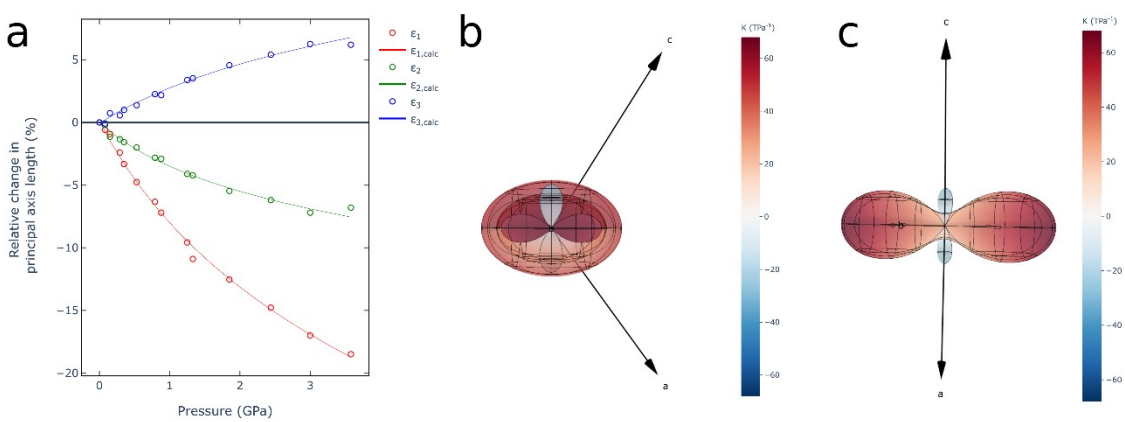

Figure S5. Relative change in length of the principal axes in function of pressure (a), and compressibility indicatrix plots (b,c) representing compressibility tensors for ETYFUM all data (0.1 MPa-3.58 GPa pressure range). The indicatrix plots are shown along crystallographic axis *b* (b), and along direction [101] (c). Positive and negative linear compressibility is marked in red and blue, respectively, in the indicatrix plots.

4. Molecular aggregation and wine rack motif geometry

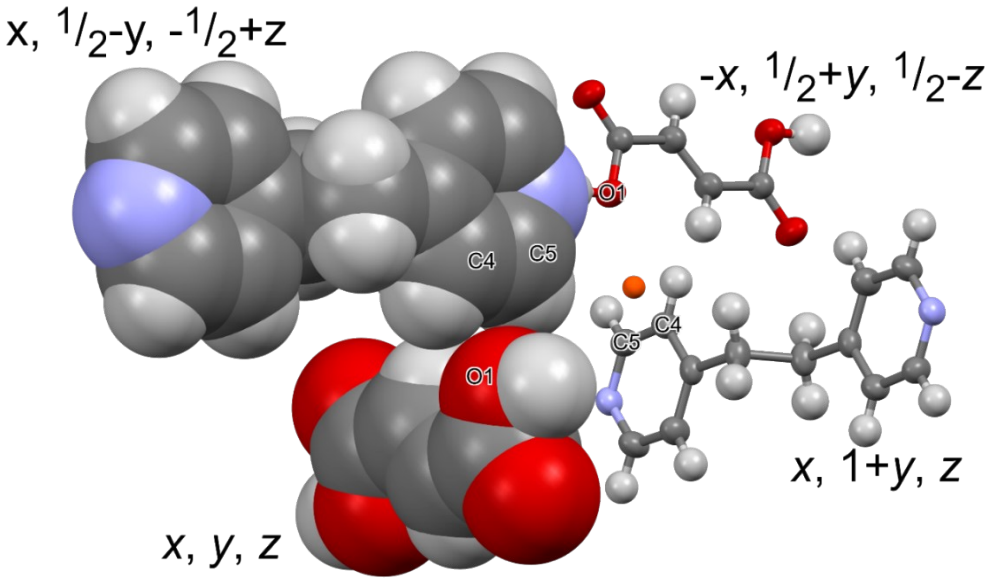

Figure S6. The respective positioning of ETY and FUM molecules at 298K/0.1 MPa, showing oxygen atom O1 interlocked between carbon atoms C4 and C5. Molecules are shown in spacefill and ellipsoid styles in program Mercury. An orange sphere represents centroid calculated for atoms O1, C4 and C5. The symmetry code for each molecule is listed next to it.

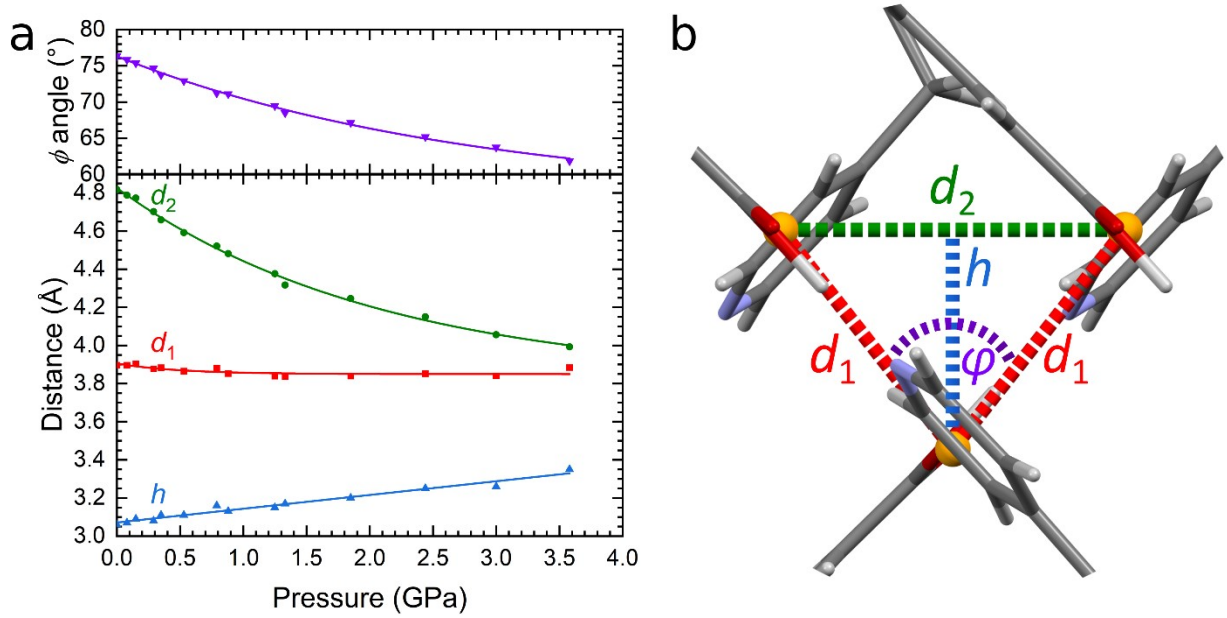

Figure S7. Pressure dependence of parameters d_1, d_2, h and φ of the triangle formed by centroids acting as hinge points (a) and fragment of ETYFUM structure (at 0.1 MPa/298 K) with the 'triangle' marked (orange centroids marking corners, red and green dashed lines marking sides and base of the triangle, respectively, height marked with blue dashed line and angle between triangle sides marked by purple arc).

Solid lines in graph in pane (a) show functions $y = a - bc^x$(where *x* is pressure in GPa, see Table S26) fitted to data measured from experimentally determined structures.

5. Negative Linear Compressibility

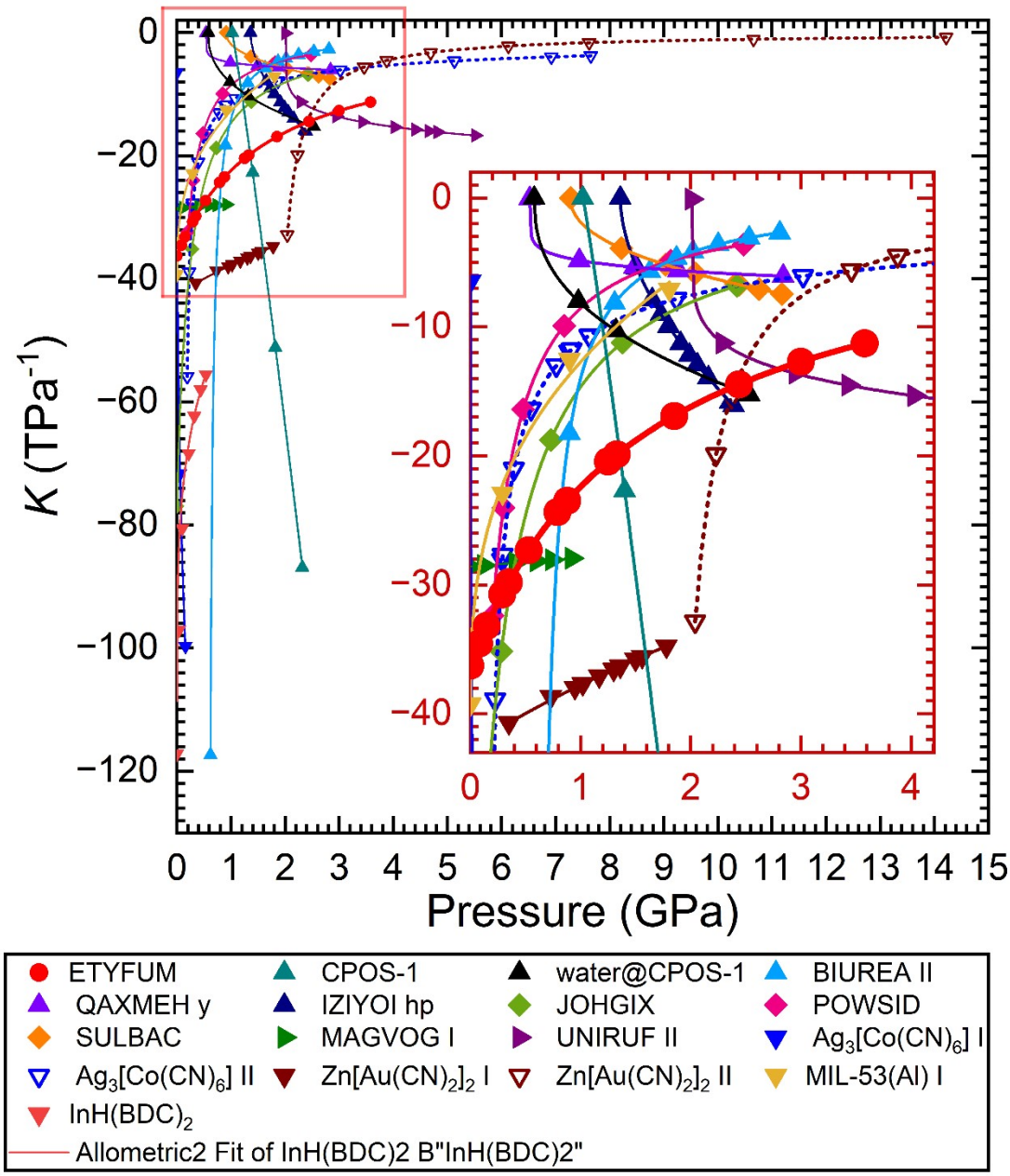

Figure S8. Pressure dependence of negative linear compressibility for selected NLC materials. The insert magnifies the 0.1 MPa-2.4 GPa pressure range for compressibility down to -46 TPa^{-1} for clearer presentation of data. Where possible materials are referenced by their REFCODES from Cambridge Structure Database (CSD)[18]. The names of the compounds are followed by information about polymorph (where applicable): yellow - yellow polymorph; hp - high-pressure polymorph; I- Phase I; II- Phase II. In case two polymorphs exhibit NLC, both are plotted in the same color but phases from higher pressure is

represented with dashed lines. Symbol shape corresponds to the type of the crystal: circle – ETYFUM; triangle - organic crystals, diamond – metal complexes, right-side triangle - inorganic-organic frameworks and coordination polymers selected from CSD datamining results; upside-down triangle – other framework materials selected from previous reports.

6. Compressibility capacity

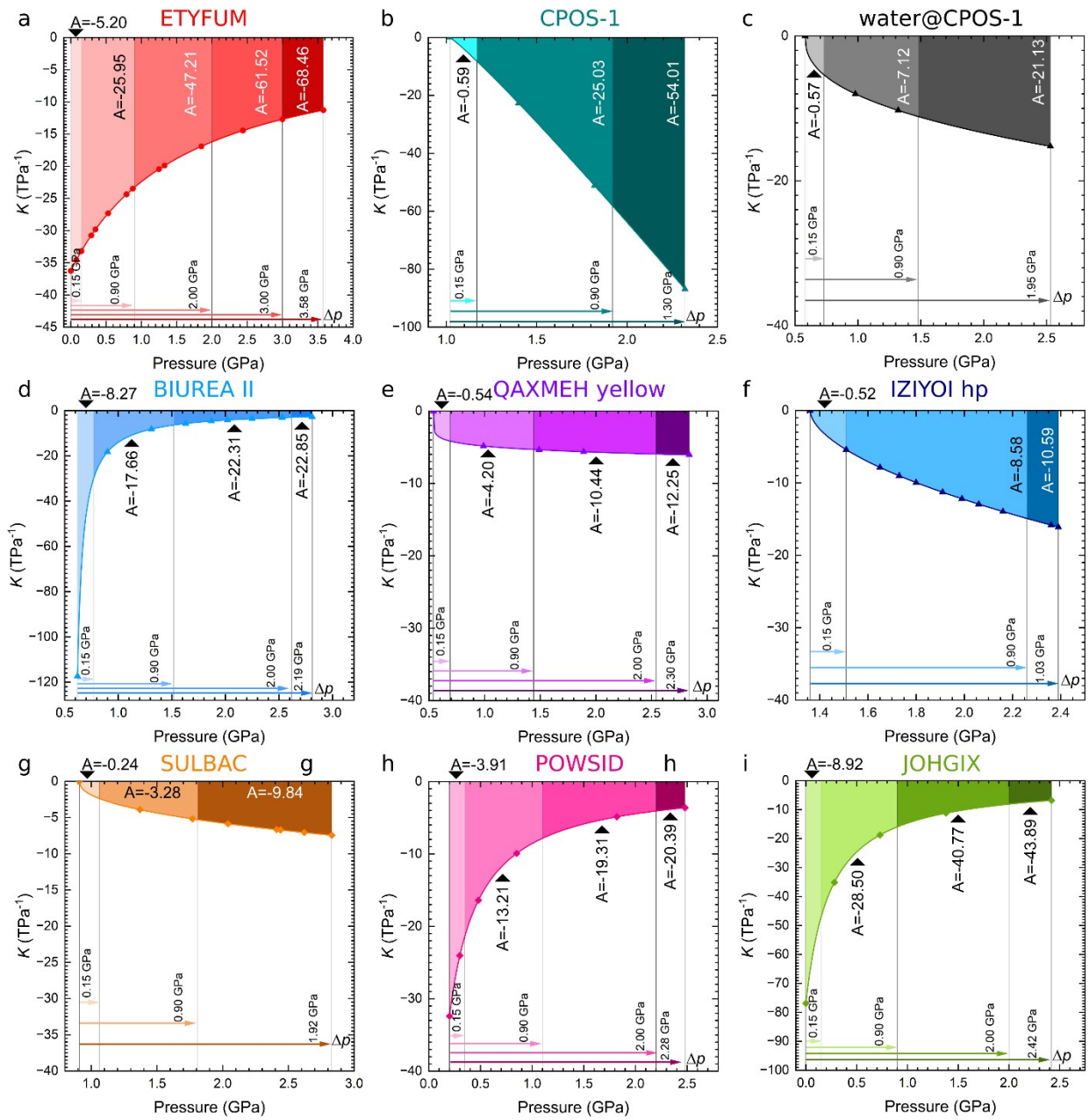

Figure S9. Evolution of compressibility with pressure for selected NLC materials (Part 1). Names of the compounds are included above the respective graphs. The names of the compounds are followed by information about polymorph (where applicable): yellow - yellow polymorph; hp - high-pressure polymorph; I- Phase I; II- Phase II. The arrows mark the Δ*p* widths for which integration was done, with the results of the integration also included in the figure (the color of the arrow corresponds to the color

of the area between function and top axis). For each compound, same p_{min} was selected for integration and only p_{max} progressively increases (the areas for different integrations overlap, with the area for wider Δp being partially covered by areas marking preceding integrations). As compressibility K is expressed in TPa^{-1} and pressure in GPa, the values included in the graphs should be multiplied by 10^{-3} to allow for unit conversion. Those corrected values can be multiplied by 10^2 to express them in %.

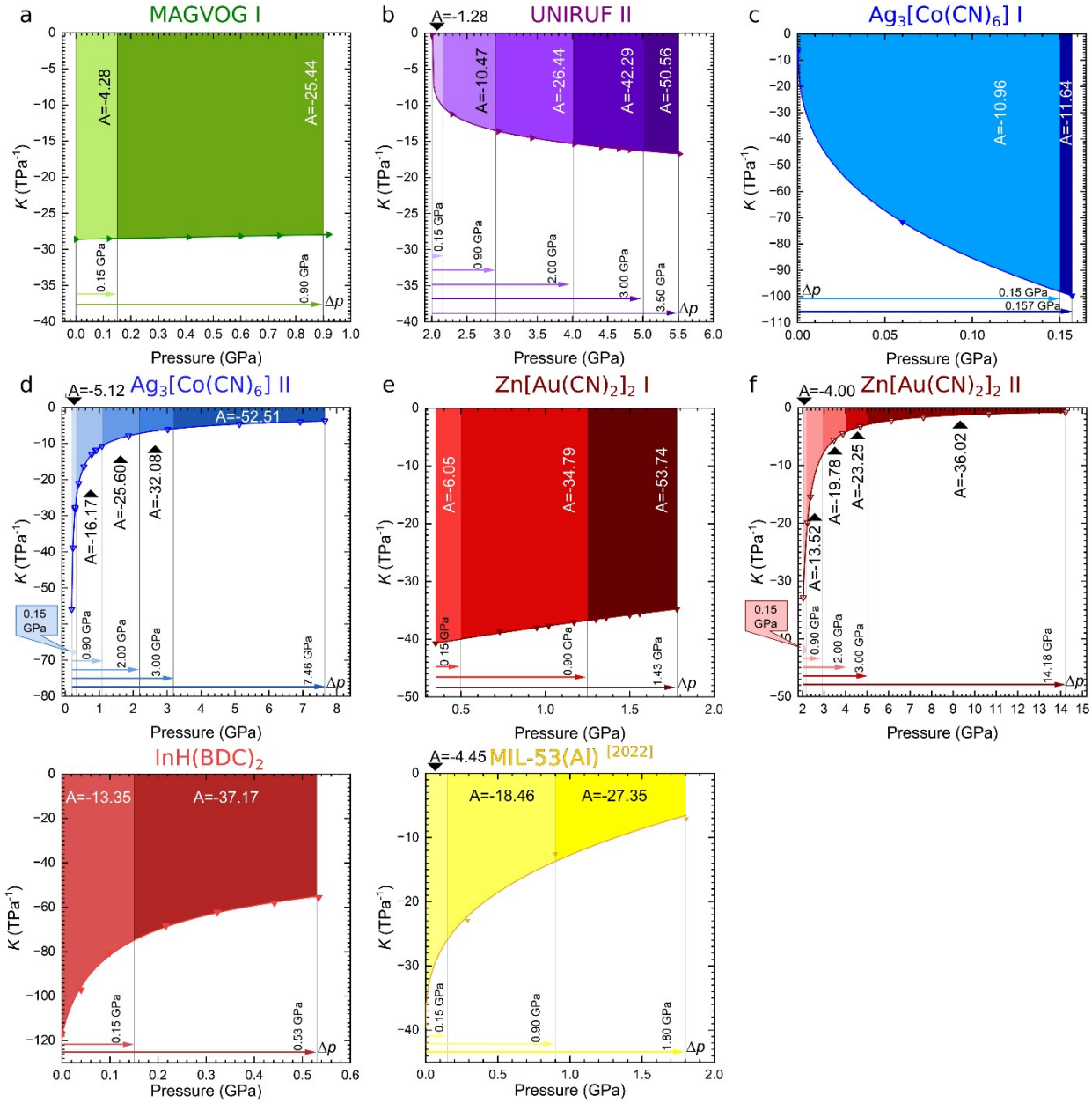

Figure S10. Evolution of compressibility with pressure for selected NLC materials (Part 2). Names of the compounds are included above the respective graphs. The names of the compounds are followed by information about polymorph (where applicable): yellow - yellow polymorph; hp - high-pressure polymorph; I- Phase I; II- Phase II. The arrows mark the Δp widths for which integration was done, with the results of the integration also included in the figure (the color of the arrow corresponds to the color of the area between function and top axis). For each compound, same p_{min} was selected for integration

and only p_{max} progressively increases (the areas for different integrations overlap, with the area for wider Δp being partially covered by areas marking preceding integrations). As compressibility K is expressed in TPa^{-1} and pressure in GPa, the values included in the graphs should be multiplied by 10^{-3} to allow for unit conversion. Those corrected values can be multiplied by 10^2 to express them in %.

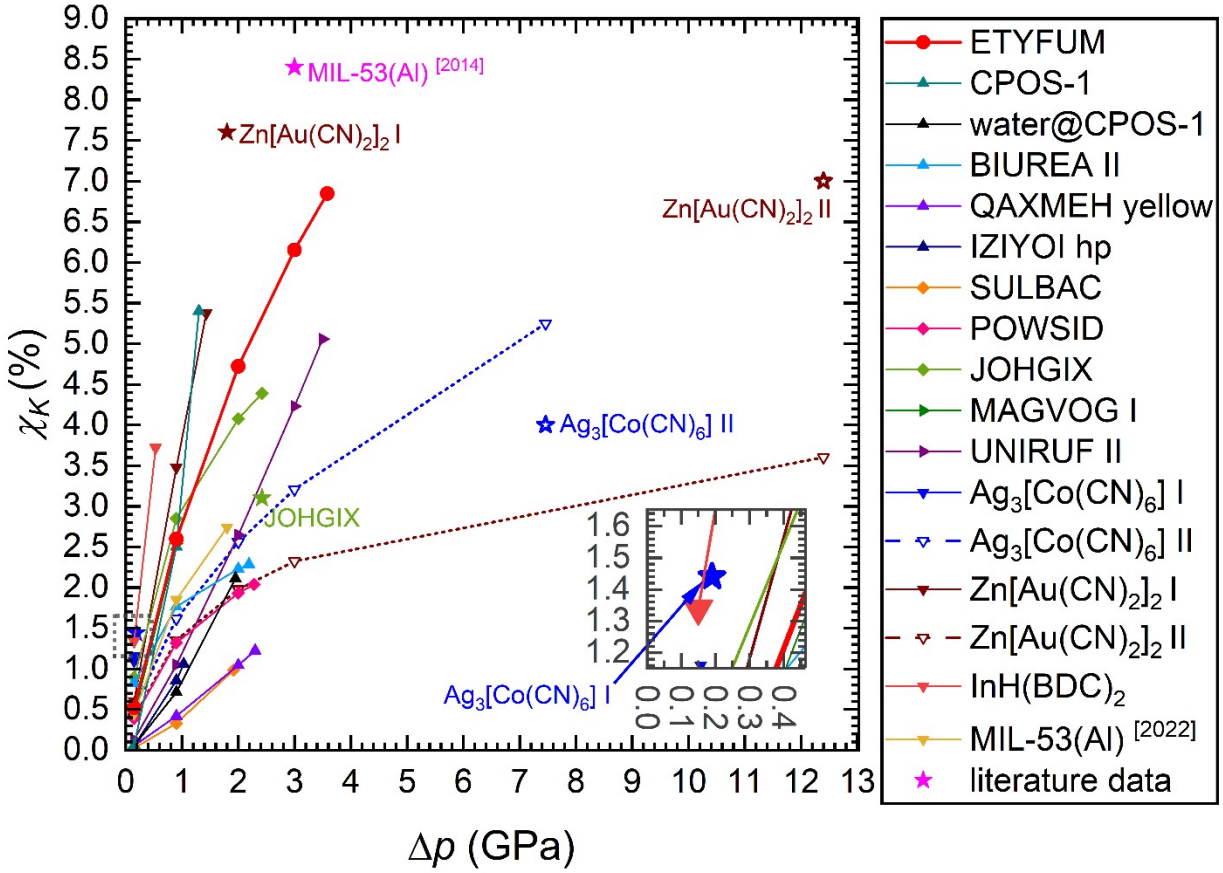

Figure S11. Evolution of compressibility capacity (χ_K) with pressure for selected NLC materials. Literature data where χ_K was listed for the complete investigated pressure range are marked with star symbols at the Δp corresponding to the width of the investigated pressure range, and are labelled with the name of the compound in corresponding color. Where possible materials are referenced by their REFCODES from Cambridge Structure Database (CSD)[18]. The names of the compounds are followed by information about polymorph (where applicable): yellow - yellow polymorph; hp - high-pressure polymorph; I- Phase I; II- Phase II. In case two polymorphs exhibit NLC, both are plotted in the same color but phases from higher pressure is represented with dashed lines. Symbol shape corresponds to the type of the crystal: circle – ETYFUM; triangle - organic crystals, diamond – metal complexes, right-side triangle - inorganic-organic frameworks and coordination polymers selected from CSD datamining results; upside-down triangle – other framework materials selected from previous reports.

References

1 CrysAlisPro, Rigaku Oxford Diffraction (version 1.171.41.93a) Rigaku Oxford Diffraction, Rigaku Oxford Diffraction 2020.
2 L. Merrill and W. A. Bassett, *Review of Scientific Instruments*, 1974, **45**, 290–294.
3 Daphne Oil 7575 Data sheet, .
4 G. J. Piermarini, S. Block, J. D. Barnett and R. A. Forman, *Journal of Applied Physics*, 1975, **46**, 2774–2780.
5 A. Budzianowski and A. Katrusiak, in *High-Pressure Crystallography*, eds. A. Katrusiak and P. McMillan, Springer Netherlands, Dordrecht, 2004, pp. 101–112.
6 K. Knížek, Kalvados https://www.fzu.cz/~knizek/kalvados/index.html.
7 OriginPro (version Version 2022b) OriginLab Corporation, Northampton, MA, USA.
8 C. F. Macrae, I. Sovago, S. J. Cottrell, P. T. A. Galek, P. McCabe, E. Pidcock, M. Platings, G. P. Shields, J. S. Stevens, M. Towler and P. A. Wood, *J Appl Cryst*, 2020, **53**, 226–235.
9 G. M. Sheldrick, *Acta Cryst A*, 2015, **71**, 3–8.
10 G. M. Sheldrick, *Acta Cryst A*, 2008, **64**, 112–122.
11 G. M. Sheldrick, *Acta Cryst C*, 2015, **71**, 3–8.
12 O. V. Dolomanov, L. J. Bourhis, R. J. Gildea, J. A. K. Howard and H. Puschmann, *Journal of Applied Crystallography*, 2009, **42**, 339–341.
13 F. Kleemiss, O. V. Dolomanov, M. Bodensteiner, N. Peyerimhoff, L. Midgley, L. J. Bourhis, A. Genoni, L. A. Malaspina, D. Jayatilaka, J. L. Spencer, F. White, B. Grundkötter-Stock, S. Steinhauer, D. Lentz, H. Puschmann and S. Grabowsky, *Chem. Sci.*, 2021, **12**, 1675–1692.
14 L. Midgley, L. J. Bourhis, O. V. Dolomanov, S. Grabowsky, F. Kleemiss, H. Puschmann and N. Peyerimhoff, *Acta Cryst A*, 2021, **77**, 519–533.
15 F. Neese, F. Wennmohs, U. Becker and C. Riplinger, *The Journal of Chemical Physics*, 2020, **152**, 224108.
16 M. J. Cliffe and A. L. Goodwin, *J Appl Cryst*, 2012, **45**, 1321–1329.
17 M. Lertkiattrakul, M. L. Evans and M. J. Cliffe, *Journal of Open Source Software*, 2023, **8**, 5556.
18 C. R. Groom, I. J. Bruno, M. P. Lightfoot and S. C. Ward, *Acta Cryst B*, 2016, **72**, 171–179.
19 Q. Zeng, K. Wang and B. Zou, *J. Am. Chem. Soc.*, 2017, **139**, 15648–15651.
20 D. Jiang, T. Wen, Y. Guo, J. Liang, Z. Jiang, C. Li, K. Liu, W. Yang and Y. Wang, *Chem. Mater.*, 2022, **34**, 2764–2770.
21 A. B. Cairns and A. L. Goodwin, *Phys. Chem. Chem. Phys.*, 2015, **17**, 20449–20465.
22 R. Dennington, T. A. Keith and ohn M. Millam, GaussView (version 6) Semichem Inc., Shawnee Mission, KS 2016.
23 M. J. Frisch, G. W. Trucks, H. B. Schlegel, G. E. Scuseria, M. A. Robb, J. R. Cheeseman, G. Scalmani, V. Barone, G. A. Petersson, H. Nakatsuji, X. Li, M. Caricato, A. V. Marenich, J. Bloino, B. G. Janesko, R. Gomperts, B. Mennucci, H. P. Hratchian, J. V. Ortiz, A. F. Izmaylov, J. L. Sonnenberg, D. Williams-Young, F. Ding, F. Lipparini, F. Egidi, J. Goings, B. Peng, A. Petrone, T. Henderson, D. Ranasinghe, V. G. Zakrzewski, J. Gao, N. Rega, G. Zheng, W. Liang, M. Hada, M. Ehara, K. Toyota, R. Fukuda, J. Hasegawa, M. Ishida, T. Nakajima, Honda, O. Kitao, H. Nakai, T. Vreven, K. Throssell, J. A. Montgomery Jr., J. E. Peralta, F. Ogliaro, M. J. Bearpark, J. J. Heyd, E. N. Brothers, K. N. Kudin, V. N. Staroverov, T. A. Keith, R. Kobayashi, J. Normand, K. Raghavachari, A. P. Rendell, J. C. Burant, S. S. Iyengar, J. Tomasi, M. Cossi, J. M. Millam, M. Klene, C. Adamo, R. Cammi, J. W. Ochterski, R. L. Martin, K. Morokuma, O. Farkas, J. B. Foresman and D. J. Fox, Gaussian (version 16 C.01) Gaussian, Inc., Wallingford CT 2016.
24 A. L. Goodwin, D. A. Keen and M. G. Tucker, *Proc. Natl. Acad. Sci. U.S.A.*, 2008, **105**, 18708–18713.
25 W. Cai and A. Katrusiak, *Nat Commun*, 2014, **5**, 4337.
26 H. H.-M. Yeung, R. Kilmurray, C. L. Hobday, S. C. McKellar, A. K. Cheetham, D. R. Allan and S. A. Moggach, *Phys. Chem. Chem. Phys.*, 2017, **19**, 3544–3549.

27 S. Sobczak, A. Półrolniczak, P. Ratajczyk, W. Cai, A. Gładysiak, V. I. Nikolayenko, D. C. Castell, L. J. Barbour and A. Katrusiak, *Chem. Commun.*, 2020, **56**, 4324–4327.
28 C. H. Woodall, C. M. Beavers, J. Christensen, L. E. Hatcher, M. Intissar, A. Parlett, S. J. Teat, C. Reber and P. R. Raithby, *Angew Chem Int Ed*, 2013, **52**, 9691–9694.
29 A. B. Cairns, J. Catafesta, C. Levelut, J. Rouquette, A. van der Lee, L. Peters, A. L. Thompson, V. Dmitriev, J. Haines and A. L. Goodwin, *Nature Materials*, 2013, **12**, 212–216.
30 J. J. Shephard, V. E. J. Berryman, T. Ochiai, O. Walter, A. N. Price, M. R. Warren, P. L. Arnold, N. Kaltsoyannis and S. Parsons, *Nat Commun*, 2022, **13**, 5923.
31 C. L. Bull, N. P. Funnell, C. J. Ridley, C. R. Pulham, P. L. Coster, J. P. Tellam and W. G. Marshall, *CrystEngComm*, 2019, **21**, 5872–5881.
32 H. J. Shepherd, T. Palamarciuc, P. Rosa, P. Guionneau, G. Molnár, J.-F. Létard and A. Bousseksou, *Angew. Chem. Int. Ed.*, 2012, **51**, 3910–3914.
33 E. L. Harty, A. R. Ha, M. R. Warren, A. L. Thompson, D. R. Allan, A. L. Goodwin and N. P. Funnell, *Chem. Commun.*, 2015, **51**, 10608–10611.
34 Y. Zhao, C. Fan, C. Pei, X. Geng, G. Xing, T. Ben and S. Qiu, *J. Am. Chem. Soc.*, 2020, **142**, 3593–3599.
35 I. E. Collings and M. Hanfland, *Molecules*, 2019, **24**, 1759.
36 W. Zieliński and A. Katrusiak, *Crystal Growth & Design*, 2014, **14**, 4247–4253.
37 A. Olejniczak, K. Krūkle-Bērziņa and A. Katrusiak, *Crystal Growth & Design*, 2016, **16**, 3756–3762.
38 E. Marelli, N. Casati, F. Gozzo, P. Macchi, P. Simoncic and A. Sironi, *CrystEngComm*, 2011, **13**, 6845–6849.
39 E. A. Kapustin, V. S. Minkov and E. V. Boldyreva, *Acta Crystallogr B Struct Sci Cryst Eng Mater*, 2014, **70**, 517–532.
40 M. Szafrański, *J. Phys. Chem. C*, 2020, **124**, 11631–11638.
41 N. E. Bogdanov, D. V. Korabel'nikov, I. A. Fedorov, B. A. Zakharov and E. V. Boldyreva, *Acta Crystallogr B Struct Sci Cryst Eng Mater*, 2022, **78**, 756–762.
42 J. M. Ogborn, I. E. Collings, S. A. Moggach, A. L. Thompson and A. L. Goodwin, *Chem. Sci.*, 2012, **3**, 3011.
43 W. Cai, A. Gładysiak, M. Anioła, V. J. Smith, L. J. Barbour and A. Katrusiak, *J. Am. Chem. Soc.*, 2015, **137**, 9296–9301.
44 I. E. Collings, R. S. Manna, A. A. Tsirlin, M. Bykov, E. Bykova, M. Hanfland, P. Gegenwart, S. Van Smaalen, L. Dubrovinsky and N. Dubrovinskaia, *Phys. Chem. Chem. Phys.*, 2018, **20**, 24465–24476.
45 I. E. Collings, M. Bykov, E. Bykova, M. G. Tucker, S. Petitgirard, M. Hanfland, K. Glazyrin, S. Van Smaalen, A. L. Goodwin, L. Dubrovinsky and N. Dubrovinskaia, *CrystEngComm*, 2016, **18**, 8849–8857.
46 Y. Yan, A. E. O'Connor, G. Kanthasamy, G. Atkinson, D. R. Allan, A. J. Blake and M. Schröder, *J. Am. Chem. Soc.*, 2018, **140**, 3952–3958.
47 A. Półrolniczak and A. Katrusiak, *Mater. Adv.*, 2021, **2**, 4677–4684.
48 A. Półrolniczak, S. Sobczak, V. I. Nikolayenko, L. J. Barbour and A. Katrusiak, *Dalton Trans.*, 2021, **50**, 17478–17481.
49 S. A. Moggach, T. D. Bennett and A. K. Cheetham, *Angewandte Chemie International Edition*, 2009, **48**, 7087–7089.
50 S. Sobczak and A. Katrusiak, *Crystal Growth & Design*, 2018, **18**, 1082–1089.